Cell-Free Full-Duplex Communication – An Overview

Diluka Galappaththige, *Member, IEEE*, Mohammadali Mohammadi, *Senior Member, IEEE,* Hien Quoc Ngo, *Fellow, IEEE,* Michail Matthaiou, *Fellow, IEEE,* and Chintha Tellambura, *Fellow, IEEE*

(Invited Paper)

***Abstract*—Cell-free (CF) architectures and full-duplex (FD) communication are leading candidates for next-generation wireless networks. The CF framework removes cell boundaries in traditional cell-based systems, thereby mitigating the inter-cell interference and improving the coverage probability. In contrast, FD communication allows simultaneous transmission and reception on the same frequency-time resources, effectively doubling the spectral efficiency (SE). The integration of these technologies, known as CF FD communication, leverages the advantages of both approaches to enhance the spectral and energy efficiency in wireless networks. CF FD communication is particularly promising due to the low-power and cost-effective FD-enabled access points (APs), which are ideal for short-range transmissions between APs and users. Despite its potential, a comprehensive survey or tutorial on CF FD communication has been notably absent. This paper aims to address this gap in the literature. It begins with an overview of FD communication fundamentals, self-interference cancellation techniques, and CF technology principles, including their implications for current wireless networks. The discussion then moves to the integration and compatibility of CF and FD technologies, focusing on channel estimation, performance analysis, and resource allocation in CF FD massive multiple-input multiple-output (mMIMO) networks, supported by an extensive literature review and case studies. The potential of combining a sub-category of CF architecture—network-assisted CF technology—with FD technology is also explored, including a detailed case study on fundamentals, performance analysis, AP operation, and mode assignments. Finally, emerging CF FD paradigms, like millimeter-wave communications, unmanned aerial vehicles, and reconfigurable intelligent surfaces, are discussed, highlighting existing contributions and unresolved issues.**

***Index Terms*—Cell-free massive multiple-input multiple-output, full-duplex, next-generation wireless networks.**

Main Nomenclature

5G	Fifth-generation
6G	Sixth-generation
ADC	Analog-to-digital converter
AP	Access point
AWGN	Additive white Gaussian noise
BS	Base station
CF	Cell-free
CLI	Cross-link interference
CPU	Central processing unit
CSI	Channel state information
DAC	Digital-to-analog converter
DL	Downlink
EE	Energy efficiency
FD	Full-duplex
FDD	Frequency-division duplex
HD	Half-duplex
IBFD	In-band full-duplex
IoT	Internet of Things
IRS	Intelligent reflecting surface
ISAC	Integrated sensing and communication
I/Q	In-phase/Quadrature phase
LoS	Line-of-sight
LSFD	Large-scale fading decoding
ML	Machine learning
MIMO	Multiple-input multiple-output
mMIMO	Massive multiple-input multiple-output
MMSE	Minimum mean square error
MRC	Maximum ratio combining
MRT	Maximum ratio transmission
MSE	Mean square error
NAFD	Network-assisted full-duplex
NLoS	Non-line-of-sight
NOMA	Non-orthogonal multiple access
OFDM	Orthogonal frequency-division multiplexing
PA	Power amplifier
PCA	Principal component analysis
PZF	Partial zero-forcing
QoS	Quality-of-service
RF	Radio-frequency
RI	Residual interference
RIS	Reconfigurable intelligent surface
RV	Random variable
RZF	Regularized zero-forcing
SE	Spectral efficiency
SI	Self-interference
SIC	Self-interference cancellation
SINR	Signal-to-interference-plus-noise ratio
SNR	Signal-to-noise ratio
TDD	Time-division duplex
UAV	Unmanned aerial vehicle
UE	User equipment
UL	Uplink
Wi-Fi	Wireless fidelity
ZF	Zero-forcing

This work was supported by a research grant from the Department for the Economy Northern Ireland under the US-Ireland R&D Partnership Programme. The work of H. Q. Ngo was supported by the U.K. Research and Innovation Future Leaders Fellowships under Grant MR/X010635/1. The work of M. Matthaiou was supported by the European Research Council (ERC) under the European Union's Horizon 2020 Research and Innovation Programme under Grant 101001331. *(Corresponding author: Diluka Galappaththige.)*

D. Galappaththige and C. Tellambura are with the Department of Electrical and Computer Engineering, University of Alberta, Edmonton, AB, T6G 1H9, Canada. (email: {diluka.lg, ct4}@ualberta.ca).

M. Mohammadi, H. Q. Ngo, and M. Matthaiou are with the Centre for Wireless Innovation (CWI), Queen's University Belfast, BT3 9DT Belfast, U.K. (email:{m.mohammadi, hien.ngo, m.matthaiou}@qub.ac.uk).

I. Introduction

THE fifth-generation (5G), beyond 5G, and sixth-generation (6G) wireless networks will be essential for all aspects of life, society, and industry, supporting technological applications like holographic telepresence, e-Health, smart environments, massive robotics, 3D unmanned mobility, augmented and virtual reality, and the Internet of Everything [1], [2]. These networks must meet diverse requirements in terms of spectral efficiency (SE), reliability, security, energy efficiency (EE), and latency [2]. Massive multiple-input multiple-output (mMIMO) systems, including co-located, distributed, and cell-free (CF) paradigms, have gained significant attention as key enabling technologies. In fact, the CF architecture, which combines the advantages of distributed antennas and co-located mMIMO, has attracted particular interest [3].

CF systems have been developed to achieve high data rates, uniform quality-of-service (QoS), and ultra-high reliability by eliminating inter-cell interference through the absence of cell borders [3]–[6]. In a conventional CF setup, numerous distributed access points (APs), connected to a central processing unit (CPU), serve all users (UEs) cooperatively. However, conventional CF systems face scalability issues, high fronthaul signaling, and computing complexity, making them problematic for large-scale networks [6]–[8]. To address this, the user-centric approach has been proposed, where each user is supported by a small number of cooperative APs, reducing the load on the CPU. This topology enhances the EE and connectivity, ensuring consistent coverage and performance across the network [6]–[8].

Full-duplex (FD) operation, which can potentially double the SE of wireless networks by eliminating the need for separate uplink (UL) and downlink (DL) channels, has gained attention with advancements in self-interference (SI) cancellation techniques [9]–[12]. SI occurs when the transmitted signal from the FD node transmitter leaks to the receiver, often overwhelming the received signal of interest, which is transmitted from another node. Effective SI mitigation is thus critical to maximize the benefits of FD. Techniques, such as propagation domain isolation, analog suppression, digital SI cancellation (SIC), and machine-learning (ML)/deep learning-based approaches have been developed for this purpose [9]–[28]. However, due to practical limitations, residual SI remains a critical factor in system performance. Despite these challenges, the FD technology is promising for next-generation wireless networks, potentially doubling the SE and addressing issues such as hidden terminals, congestion-related throughput loss, and large end-to-end delays [13].

The reduced per-AP coverage area and lower transmit power of distributed APs in CF networks make them well-suited for deploying FD transceivers, as they significantly reduce the complexity and power consumption of SI cancellation (SIC) circuits compared to co-located FD massive MIMO base stations (BSs). Additionally, lower transmit power helps mitigate inter-AP interference, thereby enhancing the network performance. CF FD networks can theoretically ensure ubiquitous connectivity for UEs operating in both UL and DL over the same frequency bands, regardless of time and location. Beyond enabling simultaneous transmissions with minimal latency, FD operation in CF networks also unlocks new opportunities for emerging technologies such as localization and sensing. By leveraging multi-cast sensing, where UL echo signals are collected at multiple APs, a cooperative sensing/localization approach can be employed, enhancing the functionality of future wireless systems.

A. Existing Survey Papers and Organization

Several separate surveys and tutorials exist for CF communication [4], [8], [29]–[35] and FD communication [12], [19], [36]–[44]. In [35], the integration of state-of-the-art and emerging technologies into CF was explored, highlighting the associated design challenges. Moreover, network-assisted CF was introduced as a novel architecture that enables simultaneous UL and DL transmissions over the same frequency bands, enhancing system flexibility. In [44], the evolutionary trajectory of cellular networks was examined, tracing their development from conventional half-duplex (HD) multi-user MIMO systems to CF FD architectures. However, they overlooked early efforts to incorporate FD technology into CF, particularly in key areas, such as channel estimation, performance analysis, signal processing, and resource allocation. Furthermore, the unique challenges posed by the FD operation at CF networks APs remain largely unaddressed. Despite the discussions in [35] and the introduction of network-assisted CF-MIMO networks in [44], no dedicated study has exclusively explored the potential of consolidating CF and FD technologies. In particular, the opportunities and challenges of CF FD networks in the contexts of millimeter-wave (mmWave) communications, unmanned aerial vehicle (UAV) communications, reconfigurable intelligent surface (RIS) deployments, and integrated sensing and communication (ISAC) remain largely unexplored. This survey is the first to do so. Reference [45] highlighted the SE and EE enhancements achieved by the integration of FD and CF, as well as corresponding challenges in future wireless networks. However, it did not fully explore recent advancements and integration challenges, leaving a significant gap in the literature. This study aims to fill that gap by comprehensively reviewing the amalgamation of FD and CF technologies.

The contributions of this paper are summarized as follows:

1) The principles of FD communication are introduced, focusing on transceiver structures and the types of SI. Classical SI mitigation approaches, including passive suppression (propagation-domain SIC) and active cancellation (analog- and digital-domain SICs), are reviewed, along with recent ML-based SI mitigation methods. Additionally, the CF technology is briefly introduced, along with its implications for both existing and future wireless networks.
2) The feasibility of merging CF and FD technologies is examined, focusing on channel estimation, performance analysis, and resource allocation in CF FD networks. An extensive literature review is provided, along with case studies using a general CF FD system configuration.
3) The paper explores CF network-assisted FD (NAFD) networks, which use HD transceivers to achieve virtual

in-band FD (IBFD) communication. A comprehensive case study delves into the basics, performance analysis, and AP operation and mode assignments.

4) Finally, remaining challenges, open issues, and emerging trends are addressed, including a review of new CF FD paradigms like mmWave communications, UAV communication, RISs, and ISAC, focusing on existing contributions and unresolved challenges.

The remainder of this paper is as follows: Section II presents an overview of FD technology, followed by a detailed discussion on the fundamentals of CF in Section III. In Section IV, we explore the application of FD within CF systems. Subsequently, Section V introduces the CF NAFD concept, offering a unified approach to CF FD and HD communication. Finally, Section VI highlights the opportunities and challenges that CF FD pose for future 6G networks, with concluding remarks provided in Section VII.

Notation: We use bold upper case letters to denote matrices and lower case letters to denote vectors. The superscripts $(\cdot)^{\mathrm{H}}$ and $(\cdot)^{-1}$ stand for the conjugate-transpose (Hermitian) and matrix inverse, respectively; $\mathbf{I}_N$ denotes the $N \times N$ identity matrix. A circularly symmetric complex Gaussian distribution having variance σ^2 is denoted by $\mathcal{CN}(0, \sigma^2)$. Moreover, $|\cdot|$ and $\|\cdot\|$ denote the absolute value and norm operators, respectively. Finally, $\mathbb{E}\{\cdot\}$ denotes the statistical expectation.

II. Full-Duplex Fundamentals

HD mode is the standard in current wireless networks, where transceivers use orthogonal channels for end-to-end transmission [46]. This means transmitting and receiving in non-overlapping time slots (time-division duplex, TDD), frequency slots (frequency-division duplex, FDD), or using distinct orthogonal spectrum-spreading codes, effectively eliminating strong SI [46]. However, the rapid growth of wireless applications demands much higher SE for next-generation systems [2]. This FD operation, which enables simultaneous transmission and reception over the same time and frequency resources, offers a promising path to meet these needs [36], [37], [40], [47]–[49]. The primary challenge for FD systems is SI – the leakage of a node's transmitted signal into its own receiver antennas. If this SI can be sufficiently canceled or suppressed to allow accurate detection of the intended low-power received signal, FD communication could theoretically double the achievable SE [36], [48].

SI is typically several orders of magnitude stronger than the desired signal, as the latter must travel a much longer distance. For example, for two transceivers (T_1 and T_2) separated by $500\,\mathrm{m}$, the desired signal from T_1's transmitter to T_2's receiver is attenuated by approximately $120\,\mathrm{dB}$, while the isolation between the transmit and receive paths on the same transceiver may only provide $15\,\mathrm{dB}$, leaving the SI about $105\,\mathrm{dB}$ stronger than the desired signal [50]. This massive power disparity increases with transceiver separation and has historically limited FD system performance, fueling the belief that FD radios are impractical. However, recent advances in efficient SIC techniques have reignited research interest, positioning FD as a key wireless enabler beyond 5G [36], [37], [40], [48].

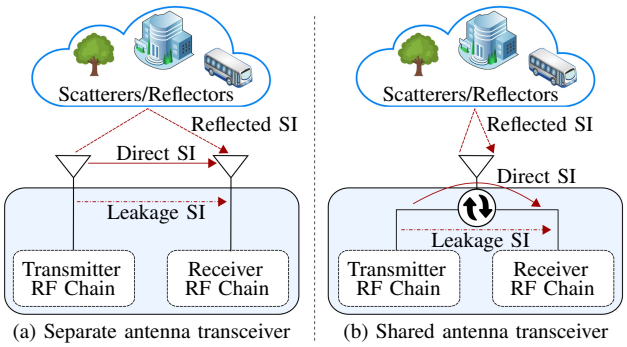

Fig. 1: The SI in separate antenna and shared antenna architectures.

There are two types of IBFD transceiver architectures: (i) separate antenna architectures, which use separate antennas for transmission and reception, and (ii) shared antenna architectures, which use the same antennas for simultaneous transmission and reception (Fig. 1) [50]. In the latter case, a circulator separates the transmission and reception paths. Regardless of the transceiver architecture, i.e., separate antennas or shared antennas, there are three distinct types of SI (Fig. 1) [51], i.e., (i) Leakage SI, (ii) Direct SI, and (iii) Reflected SI. The cumulative SI at the receiver, $x_{\mathrm{SI}}(t)$, can be mathematically expressed as

$$x_{\mathrm{SI}}(t) = \underbrace{h_{\mathrm{SI}}^{\mathtt{l}} x_t(t-\tau_l)}_{x_{\mathrm{SI}}^{\mathtt{l}}(t)} + \underbrace{h_{\mathrm{SI}}^{\mathtt{d}} x_t(t-\tau_d)}_{x_{\mathrm{SI}}^{\mathtt{d}}(t)} + \underbrace{\sum_{m=1}^{M} h_{\mathrm{SI},m}^{\mathtt{r}} x_t(t-\tau_m)}_{x_{\mathrm{SI}}^{\mathtt{r}}(t)}, \tag{1}$$

where $x_{\mathrm{SI}}^{\mathtt{l}}(t)$, $x_{\mathrm{SI}}^{\mathtt{d}}(t)$, and $x_{\mathrm{SI}}^{\mathtt{r}}(t)$ represent the leakage SI, direct SI or spillover, and reflected SI, respectively, while $h_{\mathrm{SI}}^{\mathtt{l}}$, $h_{\mathrm{SI}}^{\mathtt{d}}$, $h_{\mathrm{SI},m}^{\mathtt{r}}$ denote the respective SI channels. Here, τ_l, τ_d, and τ_m represent the associated delays, and M is the number of multi-path reflection paths from the environment. In addition, $x_t(t)$ is the transmitted signal at the transmitter antenna. In particular, to generate $x_t(t)$, the digital-to-analog converter (DAC) in the transmitter first converts the baseband data/signal, $x_b[n]$, to its analog version, $x_b(t)$, i.e., the baseband signal. The transmitter then upconverts $x_b(t)$ to the radio frequency (RF) signal, $x_u(t)$, and passes it to the power amplifier (PA) for amplification, resulting in the signal $x_t(t)$.

1) Leakage SI: This occurs on-chip or on-board in dense antenna integration and shared-antenna designs due to circulator leakage or cross-talk (e.g., due to imperfect antenna matching). This SI can be accurately characterized offline (i.e., in an anechoic chamber) and, thus, calibrated during the system design [36].

2) Direct SI: This comprises the signal propagating directly from the IBFD terminal's transmit antennas to its own receive antennas, especially in separate antenna designs. This also occurs in shared antennas due to antenna impedance mismatches. These channels are usually modeled as line-of-sight (LoS) dominated channels, e.g., Ricean [20], [52]. Due to the short distance of the direct link between the transmit and receive

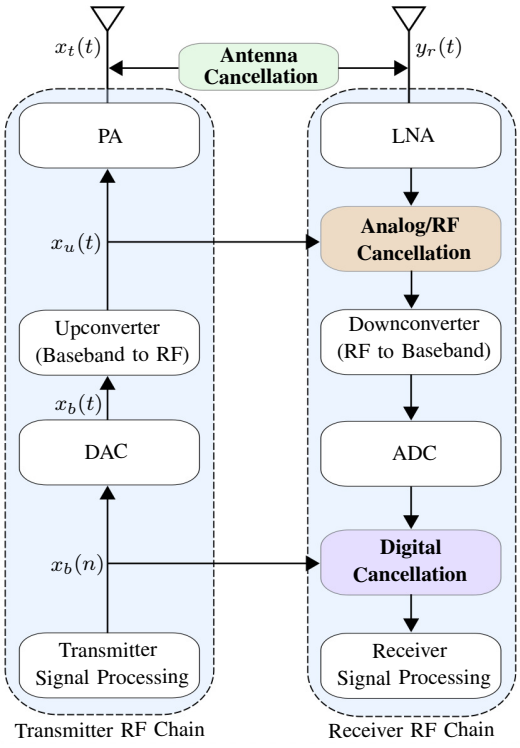

Fig. 2: A generic block diagram of an IBFD transceiver.

antennas, the direct SI power could exceed the desired signal power by up to $104\,\mathrm{dB}$ in a wireless fidelity (Wi-Fi) system [36], [53].

3) Reflected SI: This is typically due to the non-LoS (NLoS) reflections of the transmitted signal from the external environment, such as nearby objects/scatterers. Thus, the reflected SI depends on environmental effects that are changing and are inherently unpredictable. Such multi-path reflection leads to frequency-dependent/selective SI channels. These channels can be modeled empirically or analytically. The empirical models of SI channels derived from measurements are only efficient and accurate in environments with the same specific characteristics as the measurements [54]–[56]. The analytical channel models are more attractive than empirical models, and the geometry-based statistical channel model is one of the most commonly used analytical channel models [57]–[60]. These models are defined by the spatial location of the transmitter, receiver, and scatterers, which are described by the area form and spatial density of their occurrence. Typically, the reflected SI outpowers the desired received signal by $15\,\mathrm{dB}$ to $100\,\mathrm{dB}$ [53], [61]. The frequency selectivity and long propagation delay of reflected SI make the analog-circuit-domain cancellation much more challenging.

The total SI due to these three sources of SI can be substantial. Hence, effective SIC techniques are indispensable for achieving IBFD communication.

The SIC can occur at various points along the transmitter and receiver chains (Fig. 2). For example, replicating reference signals in the transmitter chain and subtracting the modified reference signal(s) in the receiver chain can remove multi-path SI. Here, additional signal delaying cancels the frequency-dependent SI, while attenuation and phase-shifting cancel the frequency-independent SI [51].

Selecting a reference signal from the transmitted signal is critical because it must capture the information and distortions caused by RF imperfections, such as phase imbalance, gain, and transmitter-generated noise and distortion. For example, the analog-to-digital converter (ADC) dynamic range will be a significant bottleneck if this is done in the digital domain at the baseband, i.e., after the ADC. In particular, the strong SI is scaled along with the input to the ADC to match their respective dynamic ranges. From the classical rule of thumb for a $10\,\mathrm{bit}$ ADC, the resultant quantization noise is $6.02 \times 10 + 1.76 = 61.96\,\mathrm{dB}$ lower than the signal at the input of the ADC [50]. If the SI is $100\,\mathrm{dB}$ higher than the desired signal, the quantization noise will be approximately $38\,\mathrm{dB}$ higher. Therefore, even if the SI is completely canceled at the ADC output, the receiver will not be able to process the desired signal.

On the other hand, the dominant nonlinearities in the PA processes cannot be eliminated if a reference signal is copied before it encounters the PA. Similarly, eliminating the SI early in the receiver's RF chain is advantageous because it reduces the demands on the receiver's front-end linearity, ability to handle large signals, and the resolutions required for the ADC. This highlights the significance of implementing SIC near the antenna, and thus, choosing a reference signal as close to the antenna as possible is preferable. However, additional SIC at the digital baseband is still required, especially to cancel the frequency-dependent SI. Furthermore, the transmitter impairments are significant compared to the received desired signal and must be reduced. Simply reducing the SI using the known transmitted symbols can result in a large residual SI. Hence, designing SIC techniques is the most essential element of implementing the revolutionary FD paradigm [9].

A. SI Mitigation

Various SIC/suppression schemes have been proposed for FD systems [9], [13]–[17]. The proposed methods employ a combination of antenna (i.e., propagation-domain), radio-frequency (RF) (i.e., analog-domain), and baseband (i.e., digital-domain) techniques, which are classified into two categories.

1) *Passive suppression:* The propagation domain SIC methods are passive and avail of physical methods to increase the propagation loss of the SI signal [13], [18]–[20]. Examples of these techniques are antenna separation, antenna cancellation, directional antennas, cross-polarization, and other techniques. Environmental reflections limit the effectiveness of cancellation. The maximum cancellation achieved in the reflective room, for example, is approximately $27\,\mathrm{dB}$ lower than in the anechoic chamber [11]. Therefore, additional cancellation (i.e., $30\,\mathrm{dB}$ to $70\,\mathrm{dB}$) is required in the analog and digital domains to reduce the SI signal level to the noise floor [19], [20].
2) *Active cancellation:* SICs in the analog and digital domains are active methods. Analog cancellation can

suppress the high-power SI caused by the ADC. It necessitates training sequence-based approaches or adaptive interference cancellation [13], [62]. Since the residual SI after the analog active cancellation is still the rate-limiting bottleneck, additional digital cancellation is required. Digital cancellation requires delays, and phase shifts between the transmitted and received signals to remove linear and nonlinear residual SI components. Thus, SI channel estimation is necessary [63].

Combining them is an option because no single analog or digital method can provide sufficient SI canceling capacity. Nonetheless, nonlinear distortions, non-ideal frequency responses of circuits, phase noise, and other inevitable hardware imperfections in practical FD transceivers may limit the SIC, leaving a significant residual SI [18], [63].

1) Propagation-Domain SIC: These techniques aim to separate the transmitter and receiver chains electromagnetically. In particular, they suppress the SI before it manifests in the receive chain circuitry by physically isolating or separating an FD node's transmit and receive antennas [10]. The primary benefit of performing SI suppression in the propagation domain is that the receiver hardware does not need to accurately process signals with a wide dynamic range [36]. Separate antenna designs achieve this through a combination of path loss, cross-polarization, and antenna directionality [11], [64]–[66], whereas shared antenna architectures use the circulator, e.g., commercially available circulators can achieve transmit-receive isolation of about $20\,\mathrm{dB}$ [50].

Separate antenna systems can increase the path loss between the transmit and receive antennas by spacing them apart and/or by placing absorptive shielding between them [11], [65], [66]. Although this is a simple technique, its effectiveness is limited by the device's form factor, i.e., the smaller the device, the less room for such an implementation. Cross-polarization provides an additional mechanism for isolating the IBFD transmit and receive antennas. For example, an IBFD terminal that transmits only horizontally polarized signals and receives only vertically polarized signals can avoid interference between them [11], [64]. Antenna directionality, on the other hand, aims to avoid interference via directional transmit and/or receive antennas by aligning the null directions [11], [65].

Even if factors like placement sensitivity and device integration hinder the performance of these techniques in practice, they can still be quite effective at suppressing the direct SI [11]. For example, reference [11] achieved a SI suppression level of $74\,\mathrm{dB}$ using commercially available hardware in an anechoic chamber setting, which is a much more accurate representation of an outdoor environment with generally fewer reflections. However, the same design performs poorly in highly reflective indoor environments, only providing $46\,\mathrm{dB}$ suppression. This is because it is sensitive to reflected SI, the channel characteristics of which are unknown when the system is designed. It is worth noting that the same issues arise in shared-antenna systems, i.e., a circulator can accurately suppress the direct SI. Yet, it cannot distinguish between the reflected SI and the desired signal.

On the other hand, dealing with reflected SI caused by nearby multi-path scattering necessitates channel-aware SI suppression methods. Transmit beamforming is one such channel-aware propagation-domain SI suppression scheme. It directs the IBFD terminal's multi-antenna transmit array by customizing the complex weights per antenna to zero the radiation pattern at each IBFD receive antenna [65], [67], [68]. However, this requires accurate knowledge of the direct and reflected SI channel gains and delays, which can be acquired either explicitly through channel estimation or implicitly through weight adaptation [36].

We point out that the aforementioned channel-aware or channel-unaware propagation-domain SI suppression techniques have a critical weakness, i.e., they may accidentally suppress the desired signal when adjusting the IBFD transmit and/or receive patterns to suppress the SI [36].

2) Analog-Domain SIC: These methods aim to suppress the SI in the analog receive-chain circuitry before the ADC. In particular, the main idea is to replicate a reference signal(s) in the transmitter chain, process it in the analog domain, and subtract the modified reference signal(s) in the receiver chain to cancel the SI. This suppression can happen before or after the downconverter and low-noise amplifier. Other possibilities include replicating the reference signal in the digital domain, adjusting the essential gain/phase/delay, and then converting it to the analog domain for SIC [10], [62], [69]. Like the propagation domain counterpart, analog domain cancellation techniques can be channel-aware or channel-unaware. Channel-unaware techniques cancel only the direct SI, whereas channel-aware techniques aim to cancel both the direct and reflected SI [11], [13], [14], [62].

The direct and reflected SI channels can be modeled in a narrowband transmission scenario as complex gains and delays between each transmit and receiver antenna pair. In this case, a single antenna IBFD transceiver with separate transmit and receiver antennas needs to adjust only a single scalar complex cancellation gain and a single delay. A channel-unaware scheme can do this once the system is designed or calibrated. On the other hand, a channel-aware design constantly adjusts this gain and delay to compensate for changes in the reflected SI channel [13], [36], [62].

The same techniques as in narrowband transmission can mitigate the direct SI if the antenna gain and phase responses are frequency-flat. However, analog-domain SIC is much more challenging because the reflected SI is generally frequency-selective due to multi-path propagation. In particular, replicating and processing a reference signal in the analog domain necessitates the adaptation of an analog filter for each transmit-receive antenna pair [36]. Another option is to digitally process the reference signal before converting it and using it in the analog domain. This makes adaptive digital filtering for reflected SIC possible, which is typically much simpler to implement in wideband orthogonal frequency-division multiplexing (OFDM) systems [69]. However, non-idealities in the receiver's analog circuit limit the cancellation accuracy.

3) Digital-Domain SIC: These methods use sophisticated digital signal processing techniques on the received signal to cancel the SI after the ADC. Working in the digital domain has the advantage of making sophisticated processing relatively easy. For example, although beamforming can be

implemented in the analog domain, it is common practice to implement it digitally due to lower circuit complexity and power consumption [18], [70]. However, the ADC's dynamic range severely limits the amount of possible SI reduction. Thus, for digital-domain methods to succeed, the propagation-domain and/or analog-domain SIC techniques must achieve sufficient SI suppression prior to the ADC. In particular, as the last line of defense against SI, these methods aim to cancel the residual SI left over from the propagation- and analog-domain approaches.

Since the transmitted signal deviates from the generated reference signal due to hardware impairments, multi-path fading, and other imperfections, subtracting the estimated signal rather than the clean signal may improve the digital cancellation capabilities significantly. In practice, digital cancellation has two main components: (i) estimating the SI channel and (ii) applying the channel estimation to the known transmitted signal to generate digital samples for subtracting the SI from the received signal [71]. Estimating the SI signal components, including leakage through the analog cancellation circuit and delayed reflections of the SI signal from the environment, is necessary to eliminate the residual SI power after analog cancellation [63]. There are two types of residual SI: linear and nonlinear. The linear SI accounts for the vast majority of SI power and can be approximated using least-squares and minimum mean square error (MMSE)-based techniques [72]. On the other hand, nonlinear SI results from nonlinear distortions in imperfect analog cancellation circuits [72]. In particular, for high SIC in the digital domain, the nonlinearity of the SI leakage channel must be precisely quantified.

4) ML-based SI Mitigation: Despite advances in classical SIC techniques, perfect RF cancellation is challenging and expensive, resulting in residual SI signals at the receiver after the RF cancellation stages, i.e., propagation-domain and analog-domain cancellations [24]. Theoretically, this residual SI can be readily canceled in the digital domain since a known transmitted baseband signal causes it. Unfortunately, this is not practically feasible, as various transceiver nonlinearities, such as baseband nonlinearities (e.g., DAC and ADC), in-phase/quadrature-phase (I/Q) imbalance, phase noise, and PA nonlinearities, contaminate the SI signal [73]–[77]. To fully cancel the SI to the level of the receiver noise floor, complicated nonlinear cancellation algorithms, often based on polynomial expansions, are necessary. For example, a parallel Hammerstein model is a commonly used nonlinear SIC method that accounts for both PA nonlinearities and I/Q imbalance [77].

Although polynomial models perform well in practice, their implementation complexity is often significant since the number of estimated parameters grows rapidly with the maximum considered nonlinearity order, whilst a large number of nonlinear basis functions must also be computed [24], [77]. On the other hand, principal component analysis (PCA), which can identify the most significant nonlinearity components of a parallel Hammerstein model, is an effective complexity-reduction technique. However, PCA-based approaches require multiplying the transmitted digital baseband samples by a transformation matrix to obtain the SIC signal, thereby introducing additional complexity. Furthermore, the high-complexity PCA procedure must be re-run whenever the SI channel undergoes a significant change.

The most recent technologies, that have received attention in academia and industry as a remedy for compensating for nonlinear effects in communications systems include ML and deep learning [24], [26], [78]. They have also been used for SIC in FD radios [21]–[28]. For example, due to their extensive nonlinear modeling capabilities, neural network-based solutions for digital SIC in FD radios have provided a favorable trade-off between computational complexity and SIC performance [24]. The basic concept is to estimate the linear and nonlinear SI separately. In particular, the linear SI is first estimated using the least squares estimation method and then subtracted from the received signal. The remaining signal, which represents the nonlinear SI, is then estimated using ML or deep learning techniques and subtracted from the received signal for final SIC [24], [26].

It is worth noting that ML-based techniques for SI mitigation operate via training models to more accurately predict and remove the SI signal than traditional methods [24]. These strategies can adapt to complex and dynamic environments, learning to model the nonlinearities and other factors that make SIC challenging. Since these approaches operate in the digital domain (usually after signal ADC), they are classified as part of digital SIC methods [24].

For more information on the fundamentals of FD communication and SIC, including classical and ML-based techniques, interested readers can refer to [45], [79] and the references therein.

III. Cell-Free Fundamentals

The advent of 5G cellular technology has significantly improved data rates and traffic volumes compared to previous cellular technologies, thus reducing data transfer latency [80]. However, it is essential to note that the benefits of these enhancements are more pronounced for users in proximity to cell centers. In contrast, users at the cell edges may still experience limitations due to inter-cell interference and handover issues inherent in cellular architectures. Therefore, while 5G presents a promising future for mobile communication, further advancements are needed to address these limitations and ensure that all users can benefit equally from this and future technologies.

In conventional cellular systems, the data source does not directly communicate with the user, which would require a high transmit power due to the user's distance. Instead, the data is sent to a nearby BS using low power, which then forwards it to a BS closer to the user. This approach allows for effective spatial reuse of the frequency spectrum and helps manage data traffic volumes. However, to handle higher traffic volumes, cellular networks often deploy more BSs in a given area, known as BS densification [31]. Unfortunately, this also increases the inter-cell interference and the frequency of handovers, resulting in traffic congestion at the cell edges. Unlike cell-center users, who experience lower interference levels and higher data rates, cell-edge users often receive

moderate data rates even in 5G networks. This is reflected in the $95\,\%$-likely user data rate, which is the minimum rate that $95\,\%$ of users can reliably achieve. However, in current 5G networks, this rate is still relatively low, indicating that many users, i.e., typically at the cell edge, do not enjoy the high performance promised by 5G [31]. To overcome these limitations, innovative solutions are needed to improve the cell-edge performance and provide better user experiences.

One potential solution to address the limitations of conventional cellular systems is to adopt a CF architecture where each user is connected to several APs, effectively treating the entire network as a single cell [81]–[90]. This approach eliminates the need for cell boundaries and significantly reduces inter-cell interference and handover issues. However, it also introduces new challenges, such as the requirement for massive fronthaul signaling for channel state information (CSI) and data sharing and high computational complexity. Several versions of this solution have been studied, including network MIMO [81]–[83], distributed MIMO [84], and coordinated multi-point [85]. To reduce fronthaul signaling and computational complexity, the network can be divided into clusters containing neighboring APs, with each cluster exchanging CSI and data only among themselves [91]–[93]. While this approach can provide some performance gains, it only addresses the interference and handover issues within the cluster boundaries, leaving the cluster edges susceptible to these limitations [94].

A user-centric network could provide a potential solution to these challenges by allowing each AP to collaborate with different sets of APs when serving different users, putting the user in control of deciding which set of APs is best for its service instead of the network [4], [5], [95]. In addition, an abundance of service antennas relative to the number of users is deployed. This approach is CF, and it has recently garnered significant research attention from the communication community [4], [5], [95], [96]. This paradigm combines the best aspects of network MIMO and mMIMO developed over the last decade [8], [97]. It involves a user-centric approach where APs cooperate to serve users based on their specific channel conditions, allowing for more efficient use of available resources and reducing inter-cell interference and handover issues.

CF communication is a novel approach that combines three previously known components: the mMIMO physical layer, ultra-dense networks with many more total number of AP antennas than users, and coordinated multipoint methods [8]. By consolidating these components, a CF system achieves a user-centric, scalable operation for large-scale deployments. This approach offers several advantages over conventional cellular networks [8]:

- It achieves smaller signal-to-noise ratio variations across the coverage area.
- It can help manage interference through joint processing at multiple APs, a capability that is very challenging in dense cellular networks.
- It can benefit from the increased SNR due to coherent transmission, allowing APs with weaker channels to participate in the transmission rather than just the AP with the best channel.

Moreover, when a large number of co-located antennas are used at an AP, two important properties emerge in CF networks: (i) Channel hardening and (ii) Favorable propagation [8]. Channel hardening occurs when beamforming transforms a fading multiantenna channel into a nearly predictable scalar channel [4], [8], [98], [99]. In other words, small-scale fading effects disappear, and time/frequency-selective channels operate essentially as additive white Gaussian noise (AWGN) channels. This simplifies resource allocation as there is no need to adjust power allocation or scheduling to small-scale fading variations. Favorable propagation implies that the channel vectors of the users are almost orthogonal. This happens due to the law of large numbers and is beneficial because there will be little interference leakage between users. In principle, these properties result from the law of large numbers [4], [8], [98], [99]. In CF, multiple AP antennas contribute to these properties. However, due to the relatively smaller number of antennas per AP compared to cellular mMIMO, a lower degree of channel hardening is expected compared to cellular networks. On the other hand, CF networks are expected to provide favorable propagation between relatively distant users, but not among those who are close together.

Since the fundamentals of CF communication have been well established, interested readers can refer to [7], [8] and the references therein for more information.

IV. Cell-free Full-Duplex Communications

CF FD communication is an emerging technology that combines the advantages of FD and CF systems to improve the SE and EE of wireless networks [100]–[106]. It is a practical and promising technology for beyond 5G networks, thanks to the low-power and low-cost FD-enabled APs.

Despite their potential benefits, the design of CF FD networks faces significant challenges compared to conventional FD systems, primarily due to severe inter-AP interference. This interference stems from the simultaneous UL and DL transmissions of a large number of APs over the same frequency band. If not properly managed, such interference can severely degrade system performance. Effective mitigation typically demands substantial fronthaul overhead to facilitate the exchange of CSI among APs. In particular, the inter-AP channels must be estimated, and the corresponding CSI either shared locally among APs for distributed interference management or forwarded to the CPU for centralized coordination.

Nevertheless, CF FD communication remains a promising paradigm owing to its inherent advantages in coverage extension, macro-diversity, and improved user fairness. The ability to decouple the user-AP association and coordinate transmissions across distributed APs offers a compelling case for its deployment. However, to fully realize its potential, robust interference management and power control techniques must be developed. Given the novelty of this research direction, only a limited number of studies have explored the performance of CF-FD networks in the literature [100]–[111]

A. Channel Estimation

Channel estimation is critical in any wireless network configuration because it improves performance, reliability,

and security [112]. In general, accurate CSI is required for various communication tasks, such as decoding, beamforming, equalization, and resource allocation. Similarly, accurate CSI is essential for signal detection, interference/SI mitigation, beamforming, and improving security and privacy in CF FD systems. Furthermore, the channel estimates assist nodes, i.e., APs/users, in detecting changes in signal characteristics caused by interference or malicious attacks and in taking appropriate measures to protect communication [112].

To estimate the CSI, wireless networks typically use pilot-based channel estimation and blind or semi-blind techniques [113], [114]. Pilot symbols are sent regularly or interleaved with data symbols to aid in channel estimation. Blind techniques, on the other hand, use the statistical properties of the received signal to estimate the CSI without the use of pilot symbols. However, due to the lack of pilot symbols, they may not achieve higher levels of accuracy (e.g., measured in terms of mean square error (MSE)) [113], [114].

Although pilots are required for accurate channel estimation in wireless systems, they come at a cost. Pilots can reduce the system's SE because they limit the time available for data transmission [115], [116]. Besides, transmitting more pilots to improve estimation accuracy can increase the system's energy consumption [115], [116]. As a result, it is essential to strike a balance between channel estimation accuracy and SE and EE to optimize the overall performance of the wireless system [115], [116]. Nonetheless, accurate channel estimation remains a critical component for improving the performance of wireless systems.

To this end, several channel estimation methodologies have been presented in the literature for CF FD systems [100], [103]–[107], [117], [118]. In particular, reference [100] presented an orthogonal pilot-based channel estimation for a generic CF FD system. It assumes that each AP has two multi-antenna arrays for transmission and reception. However, both antenna arrays can operate in transmit and receiver modes depending on the system requirement. To this end, the channels between the APs' transmit antennas and the DL users, as well as the APs' receiver antennas and the UL users, are simultaneously estimated using the MMSE methodologies used in CF systems [8]. Similarly, references [104], [117], [118] also utilized orthogonal pilot sequences to estimate the UL and DL channels using MMSE estimation.

References [103], [105]–[107] used a slightly different approach. They divide the channel training period into two slots to estimate the UL and DL channels. Specifically, the DL users first transmit their assigned orthogonal pilot sequences while the transmit antenna arrays at each AP operate in receiver mode. The APs thus estimate the DL channels using the received pilot signal through MMSE estimation. Similarly, in the next slot, the UL users transmit their pilot sequences, and the APs use the received signals at their receiver antenna arrays to estimate the UL channels. Furthermore, references [105], [106] employed a pilot sharing scheme to reduce channel training overload. In [106], the authors proposed a novel heap-based pilot assignment algorithm that can mitigate the pilot contamination's effects while reducing the computational complexity.

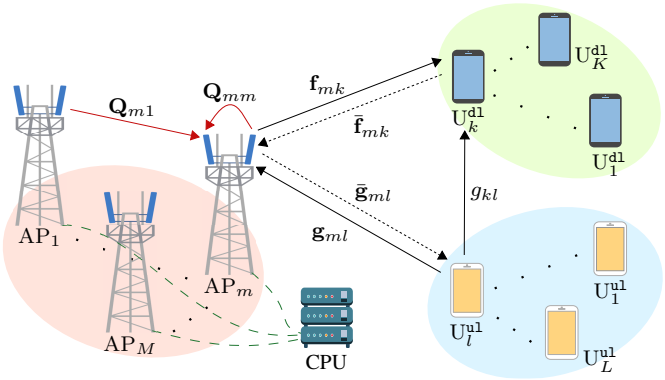

Fig. 3: A general CF FD system.

Case study and discussion: A numerical/simulation example is presented to investigate one of the CF FD channel estimation methodologies.

A CF FD system is considered consisting of M FD APs, each with $N_t \geq 1$ transmit and $N_r \geq 1$ receive antennas, K single antenna HD DL users, denoted by $\mathrm{U}_k^{\mathrm{dl}}$ for $k \in \mathcal{K}$, and L-single antenna HD UL users, denoted by $\mathrm{U}_l^{\mathrm{ul}}$ for $l \in \mathcal{L}$ (Fig. 3), where $\mathcal{K} \in \{1, \ldots, K\}$ and $\mathcal{L} \in \{1, \ldots, L\}$. The set of APs is $\mathcal{M} \in \{1, \ldots, M\}$. A CPU is assumed to connect all APs via fronthaul/fronthaul links with sufficiently large capacities. All APs simultaneously serve all DL and UL users using the same time-frequency resources. Each AP's transmit and receive antennas can operate in both transmit and receive modes. Each coherence interval includes two phases: (i) UL training and (ii) UL and DL data transmission. In particular, τ_p symbols from the coherence interval with τ_c symbols are used for UL channel estimation, while the remaining $(\tau_c - \tau_p)$ symbols are used for UL and DL data transmission.

Block flat-fading channel models are considered. Thus, during each fading block, $\mathbf{f}_{mk} \in \mathbb{C}^{N_t \times 1}$ and $\bar{\mathbf{f}}_{mk} \in \mathbb{C}^{N_r \times 1}$ denote the channel vectors from $\mathrm{U}_k^{\mathrm{dl}}$ to the mth AP transmit and receive antennas, respectively. The channels between $\mathrm{U}_l^{\mathrm{ul}}$ and the the mth AP receive and transmit antennas are denoted by $\mathbf{g}_{ml} \in \mathbb{C}^{N_r \times 1}$ and $\bar{\mathbf{g}}_{ml} \in \mathbb{C}^{N_t \times 1}$, respectively. Moreover, $h_{kl} \in \mathbb{C}$ represents the channel between $\mathrm{U}_k^{\mathrm{dl}}$ and $\mathrm{U}_l^{\mathrm{ul}}$, while $\mathbf{Q}_{mn} \in \mathbb{C}^{N_r \times N_t}$ denotes the channel between the mth AP transmit antennas and the nth AP receiver antennas. All channels are assumed to be independent quasi-static Rayleigh-faded, which remain constant during the coherence interval. A unified representation of all channels is given as

$$\mathbf{a} = \zeta_{\mathbf{a}}^{1/2} \tilde{\mathbf{a}}, \tag{2}$$

where $\mathbf{a} \in \{\mathbf{f}_{mk}, \bar{\mathbf{f}}_{mk}, \mathbf{g}_{ml}, \bar{\mathbf{g}}_{ml}, h_{kl}\}$, $\zeta_{\mathbf{a}}$ accounts for the large-scale path-loss and shadowing, and $\tilde{\mathbf{a}} \sim \mathcal{CN}(\mathbf{0}, \mathbf{I})$ captures the small-scale Rayleigh fading, which remains unchanged during one coherence interval.

During the channel training phase, each AP's transmit and receiver antennas operate in receiver mode. All UL and DL users simultaneously send their assigned pilot sequences to all APs. Let $\boldsymbol{\phi}_k^{\mathrm{dl}} \in \mathbb{C}^{\tau_p \times 1}$ and $\boldsymbol{\phi}_l^{\mathrm{ul}} \in \mathbb{C}^{\tau_p \times 1}$ be the pilot sequences transmitted by $\mathrm{U}_k^{\mathrm{dl}}$ and $\mathrm{U}_l^{\mathrm{ul}}$, respectively. These pilot sequences are pairwisely orthogonal, i.e., $(\boldsymbol{\phi}_k^{\mathrm{dl}})^{\mathrm{H}} \boldsymbol{\phi}_{k'}^{\mathrm{dl}} = 0$

TABLE I: Summary of CF FD channel estimation literature

Lit.	AP			UE			Methodology
	FD	UL	DL	FD	UL	DL	
[103]	✓	-	-	-	✓	✓	UL and DL channels are separately estimated at the APs using TDD protocol and orthogonal pilot-based MMSE estimation.
[105]	✓	-	-	-	✓	✓	
[106]	✓	-	-	-	✓	✓	
[107]	✓	-	-	-	✓	✓	
[104]	✓	-	-	-	✓	✓	UL and DL channels are simultaneously estimated at the APs using orthogonal pilot-based MMSE estimation.
[100]	✓	-	-	-	✓	✓	
[118]	-	✓	✓	-	✓	✓	
[117]	-	✓	✓	-	✓	✓	

for $k \neq k'$, $(\boldsymbol{\phi}_k^{\mathtt{dl}})^{\mathrm{H}} \boldsymbol{\phi}_l^{\mathtt{ul}} = 0$, and $(\boldsymbol{\phi}_l^{\mathtt{ul}})^{\mathrm{H}} \boldsymbol{\phi}_{l'}^{\mathtt{ul}} = 0$ for $l \neq l'$. This necessities $\tau_p \geq K+L$. Moreover, $\|\boldsymbol{\phi}_k^{\mathtt{dl}}\|^2 = 1$ for $k \in \mathcal{K}$ and $\|\boldsymbol{\phi}_l^{\mathtt{ul}}\|^2 = 1$ for $l \in \mathcal{L}$. Thus, the received signal at the mth AP transmit, $\mathbf{Y}_m^t \in \mathbb{C}^{N_t \times \tau_p}$, and receiver, $\mathbf{Y}_m^r \in \mathbb{C}^{N_r \times \tau_p}$, antennas are given as

$$\mathbf{Y}_m^t = \sqrt{\tau_p p_t} \sum_{i \in \mathcal{K}} \mathbf{f}_{mi} (\boldsymbol{\phi}_i^{\mathtt{dl}})^{\mathrm{H}} + \sqrt{\tau_p p_t} \sum_{j \in \mathcal{L}} \bar{\mathbf{g}}_{mj} (\boldsymbol{\phi}_j^{\mathtt{dl}})^{\mathrm{H}} + \mathbf{W}_m^t, \tag{3a}$$

$$\mathbf{Y}_m^r = \sqrt{\tau_p p_t} \sum_{i \in \mathcal{K}} \bar{\mathbf{f}}_{mi} (\boldsymbol{\phi}_i^{\mathtt{dl}})^{\mathrm{H}} + \sqrt{\tau_p p_t} \sum_{j \in \mathcal{L}} \mathbf{g}_{mj} (\boldsymbol{\phi}_j^{\mathtt{dl}})^{\mathrm{H}} + \mathbf{W}_m^r, \tag{3b}$$

where p_t is the average pilot transmit power at each user, while $\mathbf{W}_m^t \in \mathbb{C}^{N_t \times \tau_p}$ and $\mathbf{W}_m^r \in \mathbb{C}^{N_r \times \tau_p}$ are the AWGN matrices having independent and identically distributed (i.i.d.) $\mathcal{CN}(0, \sigma_w^2)$ elements.

By projecting (3a) and (3b) onto $\boldsymbol{\phi}_k^{\mathtt{dl}}$ and $\boldsymbol{\phi}_l^{\mathtt{ul}}$, respectively, the sufficient statistics for estimating $\mathbf{f}_{mk}$ and $\mathbf{g}_{ml}$ are

$$\mathbf{y}_{mk}^t = \mathbf{Y}_m^t \boldsymbol{\phi}_k^{\mathtt{dl}} = \sqrt{\tau_p p_t} \mathbf{f}_{mk} + \mathbf{w}_{mk}^t, \tag{4a}$$

$$\mathbf{y}_{ml}^r = \mathbf{Y}_m^r \boldsymbol{\phi}_l^{\mathtt{ul}} = \sqrt{\tau_p p_t} \mathbf{g}_{ml} + \mathbf{w}_{ml}^r, \tag{4b}$$

where $\mathbf{w}_{mk}^t = \mathbf{W}_m^t \boldsymbol{\phi}_k^{\mathtt{dl}}$ and $\mathbf{w}_{ml}^r = \mathbf{W}_m^r \boldsymbol{\phi}_l^{\mathtt{ul}}$. From (4a), the MMSE channel estimate of $\mathbf{f}_{mk}$ is obtained as

$$\begin{aligned} \hat{\mathbf{f}}_{mk} &= \mathbb{E}\{\mathbf{f}_{mk} (\mathbf{y}_{mk}^t)^{\mathrm{H}}\} \Big(\mathbb{E}\{\mathbf{y}_{mk}^t (\mathbf{y}_{mk}^t)^{\mathrm{H}}\} \Big)^{-1} \mathbf{y}_{mk}^t \\ &= c_{mk}^{\mathtt{dl}} \mathbf{y}_{mk}^t, \end{aligned} \tag{5}$$

where

$$c_{mk}^{\mathtt{dl}} = \frac{\sqrt{\tau_p p_t} \zeta_{f_{mk}}}{\tau_p p_t \zeta_{f_{mk}} + \sigma_w^2}. \tag{6}$$

Similarly, from (4b), the MMSE channel estimate of $\mathbf{g}_{ml}$ is given as

$$\begin{aligned} \hat{\mathbf{g}}_{ml} &= \mathbb{E}\{\mathbf{g}_{ml}^{\mathrm{H}} \mathbf{y}_{ml}^r\} \Big(\mathbb{E}\{\mathbf{y}_{ml}^r (\mathbf{y}_{ml}^r)^{\mathrm{H}}\} \Big)^{-1} \mathbf{y}_{ml}^r \\ &= c_{ml}^{\mathtt{ul}} \mathbf{y}_{ml}^r, \end{aligned} \tag{7}$$

where

$$c_{ml}^{\mathtt{ul}} = \frac{\sqrt{\tau_p p_t} \zeta_{g_{ml}}}{\tau_p p_t \zeta_{g_{ml}} + \sigma_w^2}. \tag{8}$$

Since $\mathbf{y}_{mk}^t$ and $\mathbf{y}_{ml}^r$ are Gaussian distributed, $\hat{\mathbf{f}}_{mk} \sim \mathcal{CN}(\mathbf{0}, \gamma_{mk}^{\mathtt{dl}} \mathbf{I}_{N_t})$ and $\hat{\mathbf{g}}_{ml} \sim \mathcal{CN}(\mathbf{0}, \gamma_{ml}^{\mathtt{ul}} \mathbf{I}_{N_r})$, where

$$\gamma_{mk}^{\mathtt{dl}} = \frac{\tau_p p_t \zeta_{f_{mk}}^2}{\tau_p p_t \zeta_{f_{mk}} + \sigma_w^2}, \tag{9a}$$

$$\gamma_{ml}^{\mathtt{ul}} = \frac{\tau_p p_t \zeta_{g_{ml}}^2}{\tau_p p_t \zeta_{g_{ml}} + \sigma_w^2}. \tag{9b}$$

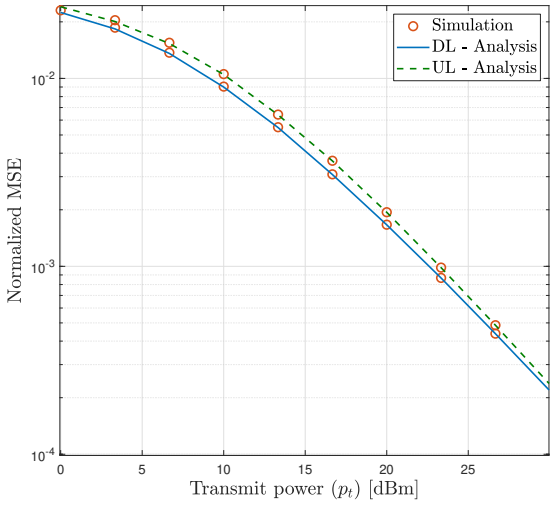

Fig. 4: Normalized MSE versus the per-user average transmit power (p_t) for $M = 16$, $N_t = N_r = 4$, $K = L = 2$, and $\tau_p = K + L$.

Next, the channel estimation errors of $\mathbf{f}_{mk}$ and $\mathbf{g}_{ml}$ are respectively given as $\mathbf{e}_{mk}^{\mathtt{dl}} \triangleq \mathbf{f}_{mk} - \hat{\mathbf{f}}_{mk} \sim \mathcal{CN}(\mathbf{0}, (\zeta_{f_{mk}} - \gamma_{mk}^{\mathtt{dl}}) \mathbf{I}_{N_t})$ and $\mathbf{e}_{ml}^{\mathtt{ul}} \triangleq \mathbf{g}_{ml} - \hat{\mathbf{g}}_{ml} \sim \mathcal{CN}(\mathbf{0}, (\zeta_{g_{ml}} - \gamma_{ml}^{\mathtt{ul}}) \mathbf{I}_{N_r})$. Owing to the property of MMSE channel estimation, $\hat{\mathbf{f}}_{mk}$, $\mathbf{e}_{mk}^{\mathtt{dl}}$, $\hat{\mathbf{g}}_{ml}$, and $\mathbf{e}_{ml}^{\mathtt{ul}}$ are independent [8].

The 3GPP UMi model is used to model the large-scale fading $\zeta_{\mathbf{a}}$ for $\mathbf{a} \in \{f_{mk}, g_{ml}, h_{kl}, Q_{mn}\}$ with $f_c = 3\,\mathrm{GHz}$ operating frequency [119, Table B.1.2.1]. Moreover, the AWGN variance is modeled as $\sigma_w^2 = 10 \log_{10}(N_0 B N_f)$ dBm, where $N_0 = -174\,\mathrm{dBm/Hz}$, $B = 10\,\mathrm{MHz}$ is the bandwidth, and $N_f = 10\,\mathrm{dB}$ is the noise figure. Moreover, the APs are uniformly distributed, while the users are randomly distributed over an area of $400 \times 400\,\mathrm{m}^2$.

The quality of channel estimators is assessed by the normalized MSE, which is defined as

$$\text{Normalized MSE} = \frac{\mathbb{E}\left\{\|\mathbf{a} - \hat{\mathbf{a}}\|^2\right\}}{\mathbb{E}\left\{\|\mathbf{a}\|^2\right\}}, \tag{10}$$

where $\mathbf{a} \in \{\mathbf{f}_{mk}, \mathbf{g}_{ml}\}$ and $\hat{\mathbf{a}} \in \{\hat{\mathbf{f}}_{mk}, \hat{\mathbf{g}}_{ml}\}$.

Figure 4 plots the average normalized MSE of the DL and UL user channel estimates as functions of the average user pilot transmit power, p_t. As in conventional CF systems, the normalized MSE of both DL and UL user channels decreases with the per-user transmit power, improving the channel

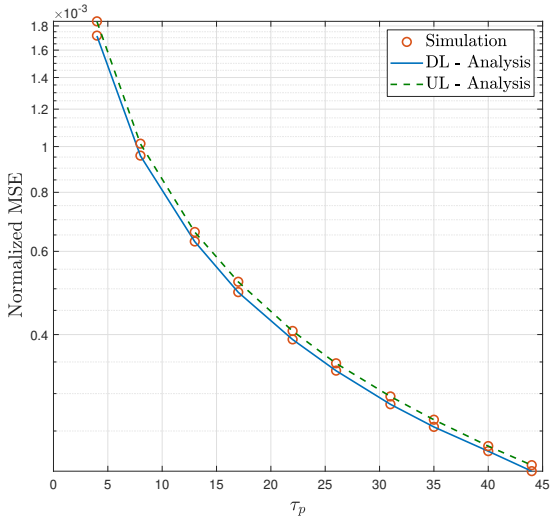

Fig. 5: Normalized MSE versus the pilot length (τ_p) for $M = 16$, $N_t = N_r = 4$, $K = L = 2$, and $p_t = 20$ dBm.

estimation quality. The key reason for this behavior is that using orthogonal pilot sequences prevents pilot contamination among DL users, DL-UL users, and vice versa. The transmit power thus improves the received signal quality at each AP.

Figure 5 shows the average normalized MSE of the DL and UL user channel estimates against the pilot length, τ_p. The result reveals that longer pilot sequences result in more accurate DL and UL user channel estimates. For example, increasing the pilot sequence length from $\tau_p = 5$ to $\tau_p = 30$ can lower the normalized MSE by $\sim 10^{0.7}$ for the UL user channels. The CF FD technical contributions can be categorized into two parts: (i) Performance analysis and (ii) Resource allocation.

B. Performance Analysis

The analytical performance evaluation is crucial in wireless networks, as it provides insights into the system's potential and limitations. These approaches can determine the throughput, delay, and error probabilities while considering practical transmission conditions and processing overheads. Developing such evaluations helps predict system requirements, estimate computational costs, and assess the accuracy needed to meet practical goals, such as ensuring the required QoS for applications. It also supports effective resource management by facilitating optimal resource allocation.

For instance, a few CF FD performance analysis frameworks are available [100], [105]. Reference [100] is the first paper to analyze a general CF FD system. The APs use conjugate beamforming and matched filtering to serve the DL and UL users, respectively, with the CSI acquired via UL training with orthogonal pilots transmitted from the users. It derived closed-form expressions for the UL and DL rates with a finite number of APs. Also, it proposed a simple power control method to mitigate the residual SI by investigating the effects of an infinite number of APs. Reference [105] investigated the SE/EE of a general CF FD system with low-resolution ADCs at the APs and DL users. The joint impact of residual SI, inter-AP interference, UL-to-DL interference, pilot contamination, and quantization noise was characterized by deriving closed-form solutions for the UL and DL rates. It was shown that increasing the number of receiving antenna arrays at the APs may compensate for the UL SE loss caused by quantization noise; however, increasing the transmit antennas is ineffective in compensating for the DL spectral loss. Furthermore, the effect of the ADCs' resolution on the operating region of the CF FD system and energy-spectral trade-offs are investigated.

Case study and discussion: We will now examine the system performance for the configuration illustrated in Fig. 3, utilizing the MMSE channel estimation outlined in Section IV-A.

DL Data Transmission: The APs construct the precoders using the channel estimates from the training phase to transmit the information signals to the DL users. By applying conjugate beamforming [120], the transmitted signal at the mth AP, $\mathbf{x}_m^{\mathtt{dl}} \in \mathbb{C}^{N_t \times 1}$, is given as

$$\mathbf{x}_m^{\mathtt{dl}} = \sqrt{p_d} \sum\nolimits_{k \in \mathcal{K}} \eta_{mk}^{1/2} \hat{\mathbf{f}}_{mk} q_k^{\mathtt{dl}}, \tag{11}$$

where p_d is the maximum normalized transmit power at each AP, η_{mk} for $m \in \mathcal{M}$ and $k \in \mathcal{K}$ is the transmit power allocation coefficient at the mth AP for $\mathrm{U}_k^{\mathtt{dl}}$, and $q_k^{\mathtt{dl}}$ is the symbols intended for $\mathrm{U}_k^{\mathtt{dl}}$, satisfying $\mathbb{E}\{|q_k^{\mathtt{dl}}|^2\} = 1$. Each AP must meet the average normalized power constraint, i.e., $\mathbb{E}\{|\mathbf{x}_m^{\mathtt{dl}}|^2\} \leq p_d$, which entails the following per-AP power constraint:

$$N_t \sum\nolimits_{k \in \mathcal{K}} \eta_{mk} \gamma_{mk}^{\mathtt{dl}} \leq 1, \quad \text{for} \quad m \in \mathcal{M}. \tag{12}$$

Next, the signal received at $\mathrm{U}_k^{\mathtt{dl}}$ is given as

$$\begin{aligned} r_k^{\mathtt{dl}} &= \sum\nolimits_{m \in \mathcal{M}} \mathbf{f}_{mk}^{\mathrm{H}} \mathbf{x}_m^{\mathtt{dl}} + \sum\nolimits_{l \in \mathcal{L}} h_{kl} x_l^{\mathtt{ul}} + w_k^{\mathtt{dl}} \\ &= \underbrace{\sqrt{p_d} \sum\nolimits_{m \in \mathcal{M}} \eta_{mk}^{1/2} \mathbf{f}_{mk}^{\mathrm{H}} \hat{\mathbf{f}}_{mk} q_k^{\mathtt{dl}}}_{\text{Desired signal}} \\ &\quad + \underbrace{\sqrt{p_d} \sum\nolimits_{m \in \mathcal{M}} \sum\nolimits_{i \in \mathcal{K}_k} \eta_{mi}^{1/2} \mathbf{f}_{mk}^{\mathrm{H}} \hat{\mathbf{f}}_{mi} q_i^{\mathtt{dl}}}_{\text{Multi-user interference}} \\ &\quad + \underbrace{\sqrt{p_u} \sum\nolimits_{l \in \mathcal{L}} \varsigma_l^{1/2} h_{kl} q_l^{\mathtt{ul}}}_{\text{UL-to-DL interference}} + \underbrace{w_k^{\mathtt{dl}}}_{\text{AWGN}}, \end{aligned} \tag{13}$$

where $\mathcal{K}_k \triangleq \mathcal{K} \backslash k$ and $w_k^{\mathtt{dl}} \sim \mathcal{CN}(0, \sigma_w^2)$ is the AWGN at $\mathrm{U}_k^{\mathtt{dl}}$. Moreover, $x_l^{\mathtt{ul}}$ is the transmitted signal at $\mathrm{U}_l^{\mathtt{ul}}$ and given as $x_l^{\mathtt{ul}} = \sqrt{p_u \varsigma_l} q_l^{\mathtt{ul}}$, where p_u is the average UL user transmit power, ς_l is the power allocation coefficient at $\mathrm{U}_l^{\mathtt{ul}}$, and $q_l^{\mathtt{ul}}$ is the message symbol of $\mathrm{U}_l^{\mathtt{ul}}$.

UL Data Transmission: UL and DL transmissions occur simultaneously at the same time-frequency block; $\mathrm{U}_l^{\mathtt{ul}}$ transmits its signal to the APs, and the transmitted signal adheres to the average transmit power constraint, $\mathbb{E}\{|x_l^{\mathtt{ul}}|^2\} \leq p_u$, which

results in the per-user power constraint as $0 \leq \varsigma_l \leq 1$. The signal received at the mth AP, $\mathbf{y}_m^{\mathtt{ul}} \in \mathbb{C}^{N_r \times 1}$, is given as

$$\begin{aligned}\mathbf{y}_m^{\mathtt{ul}} &= \sum\nolimits_{l\in\mathcal{L}} \mathbf{g}_{ml} x_l^{\mathtt{ul}} + \sum\nolimits_{n\in\mathcal{M}} \mathbf{Q}_{mn}\mathbf{x}_n^{\mathtt{dl}} + \mathbf{w}_m^{\mathtt{ul}} \\ &= \sqrt{p_u}\sum\nolimits_{l\in\mathcal{L}} \varsigma_l^{1/2}\mathbf{g}_{ml} q_l^{\mathtt{ul}} \\ &\quad + \sqrt{p_d}\sum\nolimits_{n\in\mathcal{M}}\sum\nolimits_{k\in\mathcal{K}} \eta_{nk}^{1/2}\mathbf{Q}_{mn}\hat{\mathbf{f}}_{nk} q_k^{\mathtt{dl}} + \mathbf{w}_m^{\mathtt{ul}}, \quad (14)\end{aligned}$$

where $\mathbf{w}_m^{\mathtt{ul}}$ is the AWGN vector with i.i.d. $\mathcal{CN}(0,\sigma_w^2)$ elements. To detect the message symbol transmitted by $\mathrm{U}_l^{\mathtt{ul}}$, the mth AP multiplies the received signal $\mathbf{y}_m^{\mathtt{ul}}$ with the conjugate of the channel estimate, i.e., $\hat{\mathbf{g}}_{ml}^{\mathrm{H}}$, and then sends the resulting signal to the CPU.

Since the fronthaul links connect all APs to the CPU, the inter-AP interference can be viewed as the virtual residual interference (RI) of a virtual large BS with all transmit and receive antennas collocated [100]. Hence, residual inter-AP interference can be modeled similarly to the RI in FD systems [100]. Thus, Rayleigh fading is used to model the inter-AP interference channels, i.e., $\mathbf{Q}_{mn}$ is a matrix whose elements are i.i.d. $\mathcal{CN}(0,\theta_{\mathrm{SI}}\zeta_{Q_{mn}})$, where θ_{SI} is the power of the RI at each AP after the SI suppression.

The received signal from $\mathrm{U}_l^{\mathtt{ul}}$ at the CPU is given as

$$\begin{aligned}y_{ml}^{\mathtt{ul}} &= \sum\nolimits_{m\in\mathcal{M}} \hat{\mathbf{g}}_{ml}^{\mathrm{H}}\mathbf{y}_m^{\mathtt{ul}} \\ &= \underbrace{\sqrt{p_u}\sum\nolimits_{m\in\mathcal{M}} \varsigma_l^{1/2}\hat{\mathbf{g}}_{ml}^{\mathrm{H}}\mathbf{g}_{ml} q_l^{\mathtt{ul}}}_{\text{Desired signal}} \\ &\quad + \underbrace{\sqrt{p_u}\sum\nolimits_{m\in\mathcal{M}}\sum\nolimits_{j\in\mathcal{L}_l} \varsigma_j^{1/2}\hat{\mathbf{g}}_{ml}^{\mathrm{H}}\mathbf{g}_{ml} q_j^{\mathtt{ul}}}_{\text{Multi-user interference}} \\ &\quad + \underbrace{\sqrt{p_d}\sum\nolimits_{m\in\mathcal{M}}\sum\nolimits_{n\in\mathcal{M}}\sum\nolimits_{k\in\mathcal{K}} \eta_{nk}^{1/2}\hat{\mathbf{g}}_{ml}^{\mathrm{H}}\mathbf{Q}_{mn}\hat{\mathbf{f}}_{nk} q_k^{\mathtt{dl}}}_{\text{Residual inter-AP interference}} \\ &\quad + \underbrace{\sum\nolimits_{m\in\mathcal{M}} \hat{\mathbf{g}}_{ml}^{\mathrm{H}}\mathbf{w}_m^{\mathtt{ul}}}_{\text{Noise}}, \quad (15)\end{aligned}$$

where $\mathcal{L}_l \triangleq \mathcal{L}\backslash l$.

DL SE Analysis: The DL users are unaware of the instantaneous channel coefficients without DL pilot transmission, and thus, they rely on the statistical CSI for signal decoding [8]. To this end, the signal received at $\mathrm{U}_k^{\mathtt{dl}}$ (13) is rearranged by leveraging the statistical CSI as follows:

$$\begin{aligned}r_k^{\mathtt{dl}} &= \underbrace{\sqrt{p_d}\mathbb{E}\left\{\sum\nolimits_{m\in\mathcal{M}} \eta_{mk}^{1/2}\mathbf{f}_{mk}^{\mathrm{H}}\hat{\mathbf{f}}_{mk}\right\} q_k^{\mathtt{dl}}}_{\text{Desired signal } (\mathrm{DS}_k^{\mathtt{dl}})} \\ &\quad + \underbrace{\sqrt{p_d}\left(\sum_{m\in\mathcal{M}} \eta_{mk}^{1/2}\mathbf{f}_{mk}^{\mathrm{H}}\hat{\mathbf{f}}_{mk} - \mathbb{E}\left\{\sum_{m\in\mathcal{M}} \eta_{mk}^{1/2}\mathbf{f}_{mk}^{\mathrm{H}}\hat{\mathbf{f}}_{mk}\right\}\right) q_k^{\mathtt{dl}}}_{\text{Beamforming gain uncertainty } (\mathrm{BU}_k^{\mathtt{dl}})} \\ &\quad + \underbrace{\sqrt{p_d}\sum\nolimits_{m\in\mathcal{M}}\sum\nolimits_{i\in\mathcal{K}_k} \eta_{mi}^{1/2}\mathbf{f}_{mk}^{\mathrm{H}}\hat{\mathbf{f}}_{mi} q_i^{\mathtt{dl}}}_{\text{Multi-user interference } (\mathrm{MUI}_k^{\mathtt{dl}})} \\ &\quad + \underbrace{\sqrt{p_u}\sum\nolimits_{l\in\mathcal{L}} \varsigma_l^{1/2} h_{kl} q_l^{\mathtt{ul}}}_{\text{UL-to-DL interference } (\mathrm{UDI}_k^{\mathtt{dl}})} + \underbrace{w_k^{\mathtt{dl}}}_{\text{AWGN}}. \quad (16)\end{aligned}$$

The effective noise, i.e., the addition of $\mathrm{BU}_k^{\mathtt{dl}}$, $\mathrm{MUI}_k^{\mathtt{dl}}$, $\mathrm{UDI}_k^{\mathtt{dl}}$, and AWGN, can be treated as the worst-case independently distributed Gaussian noise in the sense of the central limit theorem [8]. This approximation gives a tight achievable rate bound [8]. Assume that the users only use statistical CSI, hence, the signal-to-interference-plus-noise ratio (SINR) at $\mathrm{U}_k^{\mathtt{dl}}$ is given as

$$\mathtt{SINR}_k^{\mathtt{dl}} = \frac{|\mathrm{DS}_k^{\mathtt{dl}}|^2}{\mathbb{E}\{|\mathrm{BU}_k^{\mathtt{dl}}|^2\} + \mathbb{E}\{|\mathrm{MUI}_k^{\mathtt{dl}}|^2\} + \mathbb{E}\{|\mathrm{UDI}_k^{\mathtt{dl}}|^2\} + \sigma_w^2}. \quad (17)$$

Next, by evaluating the expectation terms in (17), the closed-form solution of the SINR at $\mathrm{U}_k^{\mathtt{dl}}$ is given in (18):

$$\mathtt{SINR}_k^{\mathtt{dl}} = \frac{p_d N_t^2 \left(\sum_{m\in\mathcal{M}} \eta_{mk}^{1/2}\gamma_{mk}^{\mathtt{dl}}\right)^2}{p_d N_t \sum_{m\in\mathcal{M}}\sum_{i\in\mathcal{K}} \eta_{mi}\zeta_{f_{mk}}\rho_{mi}^{\mathtt{dl}} + p_u\sum_{l\in\mathcal{L}} \varsigma_l\zeta_{h_{kl}} + \sigma_w^2}. \quad (18)$$

The SE of $\mathrm{U}_k^{\mathtt{dl}}$ is thus given as

$$\mathcal{S}_k^{\mathtt{dl}} = \frac{\tau_c - \tau_p}{\tau_c}\log_2\left(1 + \mathtt{SINR}_k^{\mathtt{dl}}\right), \quad (19)$$

where the pre-log factor $(\tau_c - \tau_p)/\tau_c$ captures the effective portion of the coherence interval for the data transmission.

UL SE Analysis: The CPU also uses the statistical CSI to decode the data from the UL users. Rearranging the signal received from $\mathrm{U}_l^{\mathtt{dl}}$ in (15) and following the same methodology as in the DL SE analysis, the SE of $\mathrm{U}_l^{\mathtt{dl}}$ is expressed as

$$\mathcal{S}_l^{\mathtt{ul}} = \frac{\tau_c - \tau_p}{\tau_c}\log_2\left(1 + \mathtt{SINR}_l^{\mathtt{ul}}\right), \quad (20)$$

where $\mathtt{SINR}_l^{\mathtt{ul}}$ is the $\mathrm{U}_l^{\mathtt{ul}}$ SINR at the CPU, whose closed-form solution is given in (21) at the top of the next page.

C. Resource Allocation

Spectrum, transmit power, bandwidth, and other resources are limited. Hence, sharing these resources among multiple users leads to resource allocation problems. Hence, optimal resource allocation is crucial from both theoretical and practical perspectives. Since wireless users may have different requirements and priorities, and wireless networks can be of various types (e.g., commercial networks, such as Wi-Fi and long term evolution (LTE), sensor networks, and energy harvesting networks), there is no one-size-fits-all solution. Therefore, the type of resource allocation is application-dependent. However, while some wireless application problems are amenable to standard resource allocation strategies, others need specialized solutions tailored to specific needs.

CF FD resource allocation has its challenges, particularly in managing SI and inter-AP interference, which cannot be entirely eliminated. Consequently, the residual SI must be considered when assigning wireless resources (time, power, and frequency channels) to users. Resource allocation schemes have been developed to address this issue [102]–[104], [107]–[109], [111].

Reference [102] investigated a CF FD system for improved SE and EE. The authors proposed a SE and EE maximization

$$\mathtt{SINR}_l^{\mathtt{ul}} = \frac{p_u N_r^2 \left(\sum_{m\in\mathcal{M}} \varsigma_l^{1/2} \gamma_{ml}^{\mathtt{ul}}\right)^2}{p_u N_r \sum_{m\in\mathcal{M}} \sum_{j\in\mathcal{L}} \varsigma_j \zeta_{g_{mj}} \gamma_{ml}^{\mathtt{ul}} + p_d N_t \theta_{SI} \sum_{m\in\mathcal{M}} \sum_{n\in\mathcal{M}} \sum_{k\in\mathcal{K}} \eta_{nk} \zeta_{Q_{mn}} \gamma_{ml}^{\mathtt{ul}} \rho_{nk}^{d} + \sigma_w^2 \sum_{m\in\mathcal{M}} \gamma_{ml}^{\mathtt{ul}}} \tag{21}$$

problem by jointly optimizing power control, AP-user association, and AP selection. Furthermore, the realistic power consumption model, which accounts for data transmission, baseband processing, and circuit operation, was used to characterize the EE performance. References [103], [107] studied the EE maximization of a CF FD system with limited-capacity fronthaul links via the DL and UL power control. In [103], a two-layered approach was employed, where it first formulated the optimization as a generalized convex program and then solved it either centrally or decentrally using the alternating direction method of multipliers. Reference [104] proposed a virtual FD approach for CF, where IBFD is virtually implemented by using the existing HD APs without SI-suppression hardware. It developed a mixed-integer problem to maximize the sum SE by jointly designing the AP mode assignment and power control.

Reference [108] proposed a joint beamforming design for access and fronthaul links in a user-centric network with FD fronthaul. By accounting for the power consumed by SIC at FD APs, the proposed optimization scheme maximized the network EE while ensuring fronthaul rate requirements. In [109], the UL/DL SE of a CF FD system was investigated with estimated effective DL channel, ADC/DAC impairments at the APs and the users, and spatially-correlated Ricean channels. The authors maximized the non-convex global EE metric using the block minorization-maximization technique, which decomposes the problem into several convex surrogate sub-problems. Reference [111] investigated a FD CF non-orthogonal multiple access (NOMA)-assisted space-ground integrated network, which employs spectrum sharing between the satellite and terrestrial networks to improve the SE. The authors proposed a sum-rate maximization scheme that optimizes the power allocation factors of the NOMA DL, the UL transmit power, and both the satellite and AP beamformer. Reference [121] studied the UL/DL transmit power minimization to maximize the SE and EE of a CF FD system over Ricean fading channels under SI and inter-AP interference at APs, UL-to-DL interference at DL users, and low-resolution ADCs at both APs and DL users. Table II provides a summary of the existing literature on CF FD communication.

Case study and discussion: Power allocation is now presented for the CF FD system in Fig. 3.

1) Transmit Power Control: The spatial distribution of the (UL/DL) users causes the near-far effect, which affects the achievable rates. Nonetheless, max-min transmit power control, optimal for user fairness in mitigating the near-far effect, can provide uniform QoS to all users, as in conventional CF systems. To this end, for a given realization of large-scale fading, the UL and DL power control coefficients can be found, i.e., η_{mk} and ς_l, that maximize the minimum of all UL and DL user rates, respectively, under the relevant constraints. Since the UL and DL transmissions occur concurrently, the multi-objective optimization technique must be invoked [122]. Besides, since the rates in (19) and (20) are monotonically increasing functions of their arguments, i.e., $\mathtt{SINR}_k^{\mathtt{dl}}$ and $\mathtt{SINR}_l^{\mathtt{ul}}$, they can be equivalently replaced with SINR terms in (18) and (21), respectively. By introducing a common SINR, λ, for the UL and DL users and defining the slack variables $\mu_{mk} \triangleq \eta_{mk}^{1/2}$ and $\alpha_l \triangleq \varsigma_l^{1/2}$, a multi-objective optimization problem (MOOP) is formulated as follows:

$$\mathbf{P1}: \max_{\beta_{mk},\alpha_l} \quad (\lambda_d)^{w_d}(\lambda_u)^{w_u} = \lambda_c \tag{22a}$$

$$\text{s.t} \quad \left(\mathtt{SINR}_k^{\mathtt{dl}}\right)^{w_d} \left(\mathtt{SINR}_l^{\mathtt{ul}}\right)^{w_u} \geq \lambda_c, \tag{22b}$$

$$N_t \sum_{k\in\mathcal{K}} \beta_{mk}^2 \gamma_{mk}^{\mathtt{dl}} \leq 1, \tag{22c}$$

$$0 \leq \beta_{mk} \leq 1, \tag{22d}$$

$$0 \leq \alpha_l \leq 1, \tag{22e}$$

where w_d and w_u are the priorities assigned for the DL and UL users, respectively. The main SINR constraint (22b) in $\mathbf{P1}$ is quasi-concave [5]. The underlying optimization problem is also quasi-concave [5]. Hence, $\mathbf{P1}$ is amenable to a bisection search, solving a sequence of convex feasibility problems in each iteration. **Algorithm 1** gives the details. Moreover, $\mathbf{v}_k^{\mathtt{dl}} \triangleq \left[\sqrt{N_t}\mathbf{v}_{k1}^{\mathtt{dl}}, \sqrt{\frac{p_u}{p_d}}\mathbf{v}_{k2}^{\mathtt{dl}}, \frac{\sigma_w}{\sqrt{p_d}}\right]$ and $\mathbf{v}_l^{\mathtt{ul}} \triangleq \left[\sqrt{N_r}\mathbf{v}_{l1}^{\mathtt{ul}}, \sqrt{\frac{p_d N_t \theta_{\mathrm{SI}}}{p_u}}\mathbf{v}_{l2}^{\mathtt{ul}}, \frac{\sigma_w}{\sqrt{p_u}}\mathbf{v}_{l3}^{\mathtt{ul}}\right]$, where

$$\mathbf{v}_{k1}^{\mathtt{dl}} \triangleq \left[\mu_{11}\sqrt{\zeta_{f_{1k}}\rho_{11}^{\mathtt{dl}}}, \ldots, \mu_{MK}\sqrt{\zeta_{f_{Mk}}\gamma_{mk}^{\mathtt{dl}}}\right] \in \mathbb{R}^{MK}, \tag{23a}$$

$$\mathbf{v}_{k2}^{\mathtt{dl}} \triangleq \left[\alpha_1\sqrt{\zeta_{h_{kl}}}, \ldots, \alpha_L\sqrt{\zeta_{h_{kL}}}\right] \in \mathbb{R}^{L}, \tag{23b}$$

and

$$\mathbf{v}_{l1}^{\mathtt{ul}} \triangleq \left[\alpha_1\sqrt{\zeta_{g_{11}}\rho_{1l}^{\mathtt{ul}}}, \ldots, \alpha_L\sqrt{\zeta_{g_{ML}}\gamma_{ml}^{\mathtt{ul}}}\right] \in \mathbb{R}^{ML}, \tag{24a}$$

$$\mathbf{v}_{l2}^{\mathtt{ul}} \triangleq \left[\mu_{11}\sqrt{\zeta_{Q_{11}}\rho_{1l}^{\mathtt{ul}}\rho_{11}^{\mathtt{dl}}}, \ldots, \mu_{nk}\sqrt{\zeta_{Q_{mn}}\gamma_{ml}^{\mathtt{ul}}\rho_{nk}^{\mathtt{dl}}}, \ldots, \mu_{MK}\sqrt{\zeta_{Q_{MM}}\gamma_{ml}^{\mathtt{ul}}\gamma_{mk}^{\mathtt{dl}}}\right] \in \mathbb{R}^{M^2K}, \tag{24b}$$

$$\mathbf{v}_{l3}^{\mathtt{ul}} \triangleq \left[\sqrt{\gamma_{ml}^{\mathtt{ul}}}, \ldots, \sqrt{\gamma_{ml}^{\mathtt{ul}}}\right] \in \mathbb{R}^{M}. \tag{24c}$$

Note that $\mathbf{P1}$ is inherently a MOOP as it aims to jointly optimize the UL and DL user rates, which are interdependent due to mutual interference. To address this, we employ a scalarization technique using a weighted product of the UL and DL SINR terms, i.e., $(\lambda_d)^{w_d}(\lambda_u)^{w_u}$. This formulation enables a trade-off between the two objectives while transforming the MOOP into a single-objective problem for traceability. Although this approach deviates from the traditional Pareto-optimal MOOP structure, it aligns with well-established multi-objective optimization methodologies [122].

Equal DL and UL priorities are set for max-min rates, i.e., $w_d = w_u = 1$. Equal power allocation is set at the APs,

TABLE II: Summary of CF FD performance analysis and resource allocation literature

Category	Lit.	Setup			Channel Estimation	Technical Contribution
		AP	UL UE	DL UE		
Performance analysis	[105]	FD	HD	HD	Separate	Closed-form solutions for UL/DL SE to characterize the joint effect of residual SI, inter-AP interference, UL-to-DL interference, pilot contamination, and quantization noise.
	[100]	FD	HD	HD	Simultaneous	Closed-form expressions for the UL and DL achievable rates using conjugate beamforming with a finite number of APs. A power control method to mitigate the residual SI with a large number of APs.
	[102]	FD	HD	HD	Heap-based pilot assignment	Maximizing the SE and EE by jointly optimizing power control, AP-user association, and AP selection under a realistic power consumption model.
Resource allocation	[103]	FD	HD	HD	TDD-based orthogonal pilots	Weighted sum EE maximization via DL and UL power control utilizing a two-layered approach with limited-capacity fronthaul links.
	[104]	FD	HD	HD	Simultaneous orthogonal pilots	DL and UL SE maximization via a mixed-integer optimization problem that concurrently designs the AP mode assignment and power control with a virtual FD mode at APs.
	[107]	FD	HD	HD	TDD-based orthogonal pilots	Weighted sum EE maximization through DL and UL power control and a successive convex approximation framework with limited-capacity fronthaul links.
	[108]	FD	-	HD	-	EE maximization of a user-centric network with FD fronthaul by designing beamforming for access and fronthaul links while ensuring fronthaul rate requirements.
	[109]	FD	FD		TDD-based orthogonal pilots	Global EE maximization using the minorization-maximization technique, accounting for RF impairments at the APs and UEs, ADC/DAC resolutions, and spatially-correlated Ricean channels.
	[111]	FD	HD	HD	TDD-based orthogonal pilots	Sum-rate maximization of a CF FD NOMA-assisted space-ground integrated network by optimizing the NOMA DL power allocation factors, UL transmit power, and beamforming at both the satellite and APs.
	[121]	FD	HD	HD	TDD-based orthogonal pilots	UL/DL transmit power minimization over Ricean fading channels under SI and inter-AP interference at the APs, UL-to-DL interference at DL users, and low-resolution ADCs at both APs and DL users.

i.e., $\eta_{mk} = 1/K$ for $m \in \mathcal{M}$ and $k \in \mathcal{K}$. Moreover, full power transmission at the UL users, i.e., $\varsigma_l = 1$ for $l \in \mathcal{L}$, is considered to evaluate the performance of our proposed power control method (**Algorithm 1**). Monte-Carlo simulated user SEs are also superimposed on each curve to validate the derived analytical expressions. Moreover, let $\theta_{SI} = -70\,\mathrm{dB}$.

Figures 6 and 7 plot the DL SE and the UL SE, respectively, as functions of the respective transmit powers, i.e., per-AP DL transmit power, p_d, and per-user UL transmit power, p_u. The two figures reveal that when equal power distribution is used at APs and UL users, the DL and UL users experience distinct rates. Clearly, the near-far effect caused by the spatial distribution of users and APs has a detrimental impact on the user SEs. However, with the proposed max-min power control, all the DL and UL users, regardless of their location, attain their respective common rates. The proposed scheme thus can guarantee uniform QoS for all user nodes.

Figure 8 depicts a comparison of the sum SE for FD and HD CF mMIMO as a function of the transmit power ($p_d = p_u$) and SI suppression factor (θ_{SI}). The HD CF system operates in TDD mode to facilitate the UL and DL transmission, eliminating the requirement for SIC compared to the FD counterpart. Thus, HD CF SE is independent of the SI suppression factor. The figure reveals that the FD system has a significantly higher cumulative SE than an equivalent HD system, given that the SI suppression is sufficient, i.e., $\theta_{\mathrm{SI}} \leq -40\,\mathrm{dB}$. On the other hand, with weak SI suppression, $\theta_{\mathrm{SI}} \geq -40\,\mathrm{dB}$, the SE benefits obtained by the CF FD system through the FD transmissions completely vanish. Furthermore, despite the substantial RI suppression, i.e., $\theta_{\mathrm{SI}} \leq -40\,\mathrm{dB}$, the FD sum SE does not double compared to the HD as predicted by theoretical analysis. This is primarily due to the UL-DL interference encountered by the DL user in the CF FD system, which cannot be mitigated by SI suppression at the APs.

V. Cell-Free Network-Assisted Full-Duplex Communication

While CF FD networks support simultaneous UL and DL transmissions over the same time-frequency resources, they suffer from increased interference in both directions due to concurrent transmissions. Additionally, equipping a large number of APs with FD transceivers imposes significant costs on service providers and increases the overall power consumption of the network. The increase in the power consumption is driven by the energy-hungry SIC circuits at the APs, as well as the power demands on the fronthaul links, since all APs simultaneously use these links to transmit and receive data payloads from the CPU. To address these challenges, the

Algorithm 1 : Bisection algorithm for solving **P1**.

Initialization: Select the initial values of $\lambda_{\min}$ and $\lambda_{\max}$, where $\lambda_{\min}$ and $\lambda_{\max}$ define a range of **P1**. Choose a tolerance $\epsilon > 0$.

Repeat

Step 1: Set $\lambda_c = (\lambda_{\min} + \lambda_{\max})/2$.

Step 2: Solve the following convex feasibility problem:

$$\begin{cases} \|\mathbf{v}_k^{\mathtt{dl}}\| \leq \frac{N_t}{\sqrt{\lambda_c^{wd}}} \left(\sum\limits_{m \in \mathcal{M}} \mu_{mk} \gamma_{mk}^{\mathtt{dl}} \right), \quad \text{for} \quad k \in \mathcal{K}, \\ \|\mathbf{v}_l^{\mathtt{ul}}\| \leq \frac{N_r}{\sqrt{\lambda_c^{wu}}} \left(\sum\limits_{m \in \mathcal{M}} \alpha_l \gamma_{ml}^{\mathtt{ul}} \right), \quad \text{for} \quad l \in \mathcal{L}, \\ N_t \sum\limits_{i \in \mathcal{K}} \mu_{mi}^2 \rho_{mi}^{\mathtt{dl}} \leq 1, \quad \text{for} \quad m \in \mathcal{M}, \\ 0 \leq \beta_{mk} \leq 1, \quad \text{for} \quad m \in \mathcal{M} \quad \text{and} \quad k \in \mathcal{K}, \\ 0 \leq \alpha_l \leq 1, \quad \text{for} \quad l \in \mathcal{L}. \end{cases} \tag{25}$$

Step 3: If problem (25) is feasible, then set $\lambda_{\min} = \lambda_c$, else set $\lambda_{\max} = \lambda_c$.

Until $\lambda_{\max} - \lambda_{\min} < \epsilon$.

Output: The optimized power allocation coefficients, $\eta_{mk} = \mu_{mk}^2$ for $m \in \mathcal{M}$ and $k \in \mathcal{K}$ and $\varsigma_l = \alpha_l^2$ for $l \in \mathcal{L}$.

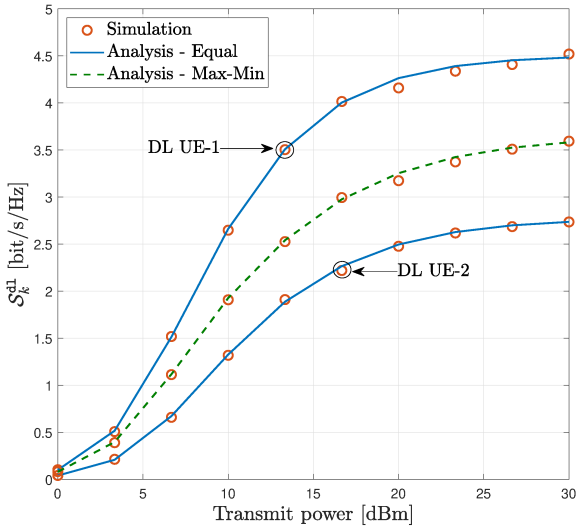

Fig. 6: DL SE versus the transmit power for $M = 16$, $N_t = N_r = 4$, $K = L = 2$, and $\tau_p = K + L$.

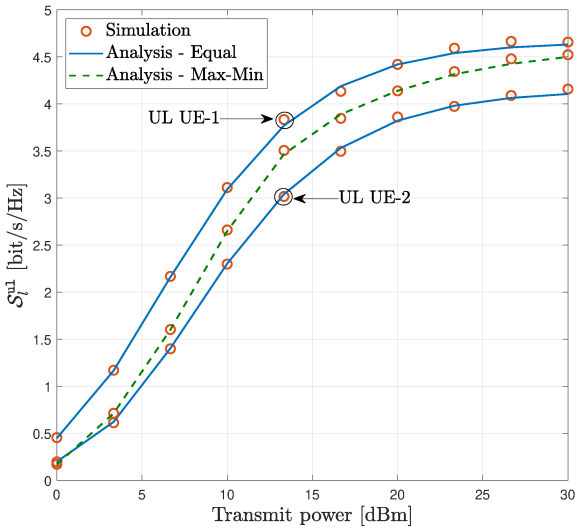

Fig. 7: UL SE versus the transmit power for $M = 16$, $N_t = N_r = 4$, $K = L = 2$, and $\tau_p = K + L$.

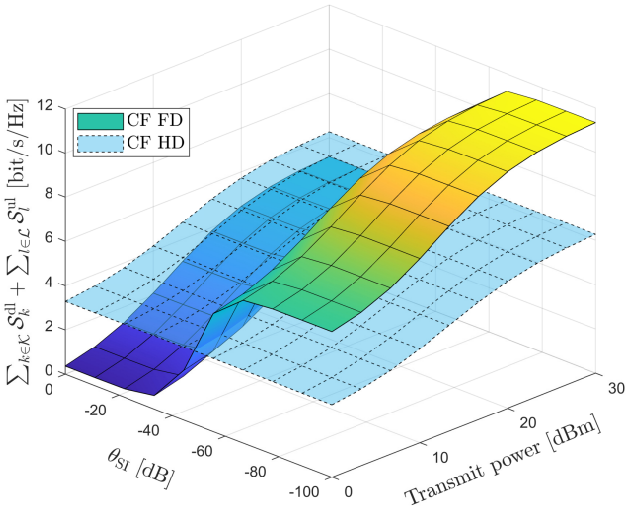

Fig. 8: A comparison of the sum SE of FD and HD CF mMIMO with transmit power allocation for $M = 16$, $N_t = N_r = 4$, $K = L = 2$, and $\tau_p = K + L$.

concept of CF NAFD was first introduced in [101], where HD APs were used to support both UL and DL transmissions. The key concept behind CF NAFD is to virtually realize the functionality of a CF FD network by using HD APs [101]. This approach offers an opportunity to efficiently manage the interference and reduce the high energy consumption associated with FD transceivers and fronthaul links while still capitalizing on the benefits of simultaneous UL and DL transmissions across the network.

A NAFD architecture shows similarities to established topologies, such as dynamic-TDD [123]–[125], dynamic UL-DL configuration in time-division LTE [126], coordinated multipoint for wireless IBFD (CoMPflex) [127], and bidirectional dynamic networks [128], which were proposed to manage the asymmetric UL-DL data traffic in wireless (cellular) networks. In dynamic TDD, a particular time slot can be assigned dynamically for reception or transmission based on the UL-DL traffic demands in each cell. However, this approach does not completely address the diverse data needs within the cells, as UEs assigned a DL (UL) time slot in a cell must wait for the UL (DL) time slot to transmit their data. Moreover, the effectiveness of the dynamic TDD is constrained by inter-BS interference and the need for strict synchronization among cells, which necessitates cell cooperation, causing significant overhead and complexity. The reasoning for implementing the dynamic UL-DL configuration in time-division Long Term Evolution is to ensure that different small cells within diverse cellular networks can support transmission in opposite direc-

tions [126]. CoMPflex, which is motivated by the coordinated multipoint concept in cellular networks, involves emulating an FD BS and using two spatially separated and coordinated HD BSs [127]. In bidirectional dynamic networks, the number of UL and DL remote radio heads is adjusted flexibly to facilitate simultaneous UL and DL communications [128].

In this context, NAFD systems offer several advantages over the conventional CF FD counterparts:

- The NAFD framework eliminates the SI within the APs, simplifying the transceiver design and avoiding the need for power-hungry SIC circuits.
- Some APs will handle UL transmission, while others will manage DL transmission, significantly reducing the fronthaul data traffic and associated energy consumption.
- The flexible adjustment of the UL and DL modes at the HD APs can efficiently cope with the inter-AP interference (a main bottleneck in CF FD systems) and, at the same time, can accommodate the increasing time-varying traffic asymmetry between the UL transmission and DL reception for 6G wireless.

These benefits have driven the application of the NAFD concept in CF systems to enable simultaneous UL and DL communications on the same frequency band.

A. Channel Estimation

To fully leverage the benefits of CF NAFD systems, accurate CSI is essential at both the CPU and terminals, to address the following aspects:

- The CPU requires CSI between the APs and terminals to design beamforming and receivers. This CSI can be obtained through pilot training under the TDD protocol, similar to conventional FD and HD CF networks.
- In NAFD-distributed massive MIMO systems, the simultaneous DL transmission and UL reception cause inter-AP interference, as the DL transmissions interfere with the UL reception. This interference remains the primary factor limiting the UL SE. Therefore, effective interference cancellation is essential for enhancing the UL SE in NAFD-distributed mMIMO systems. To this end, the estimation of the interference channel matrix between the DL-APs and UL APs is necessary.

Although the two CSI requirements mentioned are similar to those in conventional CF FD networks, there is a key distinction in NAFD systems from a channel estimation perspective. In CF NAFD systems, each terminal is usually served by a subset of nearby APs, weakening the channel hardening effect. Consequently, the DL terminals must estimate the CSI between themselves and the DL-APs directly, rather than depending on statistical CSI.

Li *et al.* [129] proposed a method to estimate the effective CSI-specifically, the inner products of beamforming and channel vectors-through a beamforming training scheme. This approach allows the CPU to estimate the effective CSI between the DL APs and UL APs, while the DL users can estimate the effective CSI between DL APs and themselves. Under this approach, they derived closed-form expressions for the UL and DL achievable rates with various receivers and beamforming strategies. Based on these expressions, they developed an efficient power allocation scheme that depends only on slowly varying large-scale fading, framed within a multi-objective optimization perspective. Note that the channel estimation proposed in [129] applies to systems with fixed AP modes. However, in dynamic NAFD systems, where the AP operation mode is designed based on UL and DL traffic, the inter-AP DL-to-UL channel estimation method in [101] becomes infeasible.

B. Performance Analysis

In [101], the SE of a CF NAFD network was analyzed for imperfect CSI and spatial correlations. By applying large-dimensional random matrix theory, deterministic equivalents for the sum rate were derived for both UL, using an MMSE receiver, and DL, employing regularized zero-forcing (RZF) and zero-forcing (ZF) precoders. The authors identified inter-AP interference (between DL and UL APs) and inter-user interference (UL-to-DL interference) as the primary bottlenecks in system design. In a static scenario, where the APs have fixed operational modes (either UL or DL), they assumed that inter-AP DL-to-UL channels could be estimated using pilot signals with minimal overhead due to the quasi-static nature of the links. To mitigate the UL-to-DL interference, they proposed a user scheduling scheme.

In [101], a fixed network configuration for APs was conceived, where certain APs are designated for UL transmission and others for DL transmission. However, in dynamic scenarios with time-varying traffic asymmetry between DL transmission and UL reception, static configurations limit the full potential of the NAFD concept. In these cases, dynamically adjusting AP operation modes to balance UL and DL transmissions would better harness NAFD's advantages. To address this shortcoming, the authors in [130] developed a comprehensive performance analysis framework under dynamic AP mode selection, offering both SE and EE analysis. They derived closed-form expressions for the UL and DL SE, assuming maximum ratio combining (MRC) and maximum ratio transmission (MRT) processing at the APs and DL UEs, while accounting for large-scale fading decoding (LSFD) coefficients in the UL. Additionally, they introduced a total power consumption model that incorporates the fronthaul power consumption.

C. Resource Allocation

Selecting the operation mode of APs (i.e., UL or DL) introduces an additional degree of freedom in NAFD systems compared to their FD counterparts. As a result, beyond the design parameters in CF FD systems—such as power control at the APs and UL users, and LSFD design at the CPU—the operation mode of the APs can also be optimized to meet the network requirements. Recent studies revealed that inter-AP interference becomes more manageable under a flexible UL/DL operation mode assignment at the HD APs. Zhu *et al.* [131] proposed a duplex mode selection algorithm based on parallel successive convex approximation, along with a reinforcement learning algorithm based on Q-learning, aiming

at maximizing the user sum rate. Chowdhury *et al.* [117] formulated the AP-scheduling problem as one of maximizing the sum UL-DL SE, by considering MRT/RZF precoding in the DL and MRC/MMSE in the UL based on the locally estimated channels. They proposed a greedy algorithm for dynamic AP-scheduling, where, at each step, the transmission mode of the AP that maximizes the incremental SE is added to the already scheduled AP-subset. Moreover, an iterative pilot allocation algorithm, based on locally estimated channel statistics at the APs, was developed. Sun *et al.* [132] proposed a "preallocation—optimization" mechanism for AP duplex mode optimization, where the preallocation part and the optimization part can help CF NAFD networks effectively handle the time-varying active UEs and network load in massive Internet of Things (IoT) scenarios. The preallocation part involves a network load prediction algorithm based on an autoregressive integrated moving average model, ensuring accurate load forecasting and efficient preallocation of resource blocks. In the optimization part, deep reinforcement learning-based and hierarchical reinforcement learning-based AP duplex mode optimization algorithms were developed to solve the multi-objective optimization problem of AP mode optimization. While the proposed algorithms offer improved performance compared to fixed duplex mode networks, some users' UL and DL SE are still compromised due to inefficient resource allocation.

The flexibility of NAFD design has been leveraged for secure transmission. Specifically, Xia *et al.* [133] focused on the joint design of transmit information vectors, artificial noise covariance matrices, AP mode selection vectors, and receiver vectors. Their goal was to maximize the secure DL and UL transmission rates while adhering to the sum transmission power constraints at the APs and UL users.

Another line of research has integrated QoS requirement constraints for UL and DL users into the AP mode assignment problem, making the associated optimization challenge more complex [130], [134]–[136]. More specifically, Xia *et al.* [134] considered the SE maximization problem in NAFD systems, where the APs operate in either FD mode or HD mode. By considering the QoS requirements of both the UL and DL users, along with fronthaul capacity constraints, they investigated the joint user selection and transceiver design. Xia *et al.* [135] addressed the EE maximization problem for a CF system with NAFD, considering QoS requirements, transmit power constraints, fronthaul capacity constraints, and energy harvesting constraints. In [134], [135], the operation mode of the APs is fixed, leaving the potential of dynamic network configuration unexplored.

Zhu *et al.* [136] proposed a load-aware dynamic mode selection scheme for the APs, aiming to maximize the UL-DL sum-rate of the network while considering the per-user traffic load. They investigated centralized Q-learning and distributed multi-agent Q-learning algorithms with varying complexities, demonstrating that the former is more suitable for real-world applications due to its smaller storage unit and lower complexity. The proposed algorithms in [134]–[136] rely on instantaneous CSI at the APs and CPU, thereby imposing high overhead and complexity on the system. To tackle this issue, Mohammadi *et al.* [130] proposed a joint AP mode assignment, power control, and LSFD design algorithm to maximize the SE and EE. Their results in [130] confirmed that by optimizing the operation mode at the APs, the EE of CF NAFD systems achieves up to a two-fold improvement over CF FD systems. Vu *et al.* [137] proposed a multipair decode-and-forward CF NAFD relaying system, where the APs with a DL mode serve destination nodes and those with a UL mode serve source nodes, at the same time. A joint optimization approach to design the AP mode assignment, power control, and LSFD weights was proposed, which maximizes the sum SE of transmission pairs, under per-pair SE requirements.

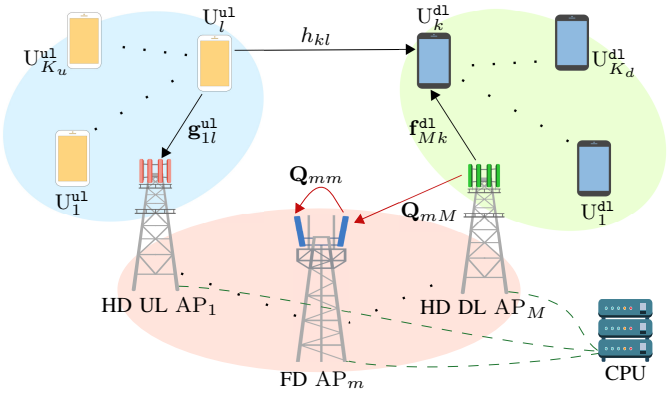

Fig. 9: CF NAFD system with HD and FD APs.

Building on the CF NAFD concept, AP mode selection has been incorporated into SWIPT-enabled CF systems [138], [139] and CF surveillance networks [140]. In these scenarios, two distinct groups of APs are designated to carry out separate functions simultaneously over the same time-frequency resources.

Case study and discussion: Consider a CF NAFD system consisting of M APs serving L UL UEs and K DL UEs, as illustrated in Fig. 9. We define the sets $\mathcal{M} \triangleq \{1, \ldots, M\}$, $\mathcal{K} \triangleq \{1, \ldots, K\}$ and $\mathcal{L} \triangleq \{1, \ldots, L\}$ as the collections of indices for the APs, DL UEs, and UL UEs, respectively. Each AP is connected to the CPU via a high-capacity fronthaul link. The DL and UL transmissions occur within the same time-frequency block, facilitated by both HD and IBFD APs. Each UE is equipped with a single antenna, while each AP has N transmit and N receive RF chains. The HD APs are dynamically assigned as DL APs or UL APs to support the respective transmissions.

In Fig. 9, the three ellipses represent different groups of network nodes for clarity. In particular, the blue ellipse encloses the UL UEs, which communicate with the UL APs. The green ellipse represents the DL UEs, which receive data from the DL APs. The red ellipse groups all APs, including the FD APs and HD APs. These visual groupings illustrate the network topology and interactions between different components, thereby enhancing the understanding of the system architecture.

The channel coefficient vector between the k-th DL UE,

TABLE III: Summary of CF NAFD literature

Category	Lit.	AP			UE			Technical Contribution
		FD	UL	DL	FD	UL	DL	
Performance Analysis	[101]	-	✓	✓	-	✓	✓	Sum-rate analysis for UL with MMSE receiver and DL with RZF and ZF precoders under fixed AP mode of operation.
	[130]	-	✓	✓	-	✓	✓	SE and EE with MRC/MRT processing under flexible AP modes of operation.
Channel Estimation	[129]	✓	✓	✓	-	✓	✓	Beamforming training scheme to estimate the effective CSI between the DL APs and UL APs at CPU as well as effective CSI between DL APs and DL users.
Resource Allocation	[117]	-	✓	✓	-	✓	✓	Development of a greedy-based AP mode selection algorithm for sum UL-DL SE maximization.
	[131]	-	✓	✓	-	✓	✓	AP duplex mode selection for sum-rate maximization with successive convex approximation and a reinforcement learning algorithm.
	[132]	-	✓	✓	-	✓	✓	AP duplex mode optimization, aiming to address the dynamic massive IoT scenarios and achieve a balance between SE and resource utilization.
	[133]	✓	✓	✓	-	✓	✓	Joint AP duplex mode and transceivers optimizing to maximize the overall secrecy SE with artificial noise transmission.
	[134]	✓	✓	✓	-	✓	✓	Maximizing the SE and number of serving UEs under the QoS requirements of UL and DL UEs, with fixed AP mode of operation.
	[135]	✓	✓	✓	-	✓	✓	Joint strategy of EH, fronthaul compression, and CLI cancelation to maximize the EE under fixed AP mode of operation.
	[136]	-	✓	✓	-	✓	✓	Load-aware dynamic mode selection scheme of APs based on centralized Q-learning and distributed multi-agent Q-learning method.
	[130]	-	✓	✓	-	✓	✓	Joint AP mode selection, power control, and LSFD design to maximize SE and EE.
	[137]	-	✓	✓	-	✓	✓	Multipair decode-and-forward CF NAFD relaying system.

$\mathrm{U}_k^{\mathtt{dl}}$, ($l$-th UL UE, $\mathrm{U}_l^{\mathtt{ul}}$) and the m-th AP, $\mathbf{f}_{mk}^{\mathtt{dl}} \in \mathbb{C}^{N\times 1}$ ($\mathbf{g}_{ml}^{\mathtt{ul}} \in \mathbb{C}^{N\times 1}$), $\forall k \in \mathcal{K}$, $l \in \mathcal{L}$, $m \in \mathcal{M}$, is modeled as $\mathbf{f}_{mk}^{\mathtt{dl}} = \sqrt{\zeta_{f_{mk}}^{\mathtt{dl}}}\tilde{\mathbf{f}}_{mk}^{\mathtt{dl}}$, ($\mathbf{g}_{ml}^{\mathtt{ul}} = \sqrt{\zeta_{g_{ml}}^{\mathtt{ul}}}\tilde{\mathbf{g}}_{ml}^{\mathtt{ul}}$), where $\zeta_{f_{mk}}^{\mathtt{dl}}$ ($\zeta_{g_{ml}}^{\mathtt{ul}}$) is the large-scale fading coefficient and $\tilde{\mathbf{f}}_{mk}^{\mathtt{dl}} \in \mathbb{C}^{N\times 1}$ ($\tilde{\mathbf{g}}_{ml}^{\mathtt{ul}} \in \mathbb{C}^{N\times 1}$) is the small-scale fading vector whose elements are i.i.d. $\mathcal{CN}(0,1)$ random variables (RVs). The channel gain between the UL UE l to the DL UE k is denoted by h_{kl}. It can be modeled as $h_{kl} = (\zeta_{h_{kl}}^{\mathtt{du}})^{1/2}\tilde{h}_{kl}$, where $\zeta_{h_{kl}}^{\mathtt{du}}$ is the large-scale fading coefficient and $\tilde{h}_{kl}$ is a $\mathcal{CN}(0,1)$ RV. Finally, the interference links among the APs are modeled as Rayleigh fading channels. Let $\mathbf{Q}_{mi} \in \mathbb{C}^{N\times N}$, $i \neq m$, be the channel matrix from AP m to AP i, $\forall m, i \in \mathcal{M}$, whose elements are i.i.d. $\mathcal{CN}(0, \zeta_{Q_{mi}})$ RVs. Here, $\mathbf{Q}_{mm}, \forall m$ denotes the SI channel at the IBFD APs, whose elements are i.i.d. $\mathcal{CN}(0, \zeta_{Q_{mm}} \triangleq \theta_{\mathrm{SI}})$ RVs.

DL Data Transmission: The signal received at $\mathrm{U}_k^{\mathtt{dl}}$ is

$$y_k^{\mathtt{dl}} = \sqrt{\rho_d}\sum\nolimits_{m\in\mathcal{M}} a_m\mu_{mk}\left(\mathbf{f}_{mk}^{\mathtt{dl}}\right)^{\mathrm{H}}\mathbf{v}_{mk}^{\mathtt{dl}}s_k^{\mathtt{dl}} + \sqrt{\rho_d}\sum\nolimits_{m\in\mathcal{M}}\sum\nolimits_{k'\in\mathcal{K}\setminus k} a_m\mu_{mk'}\left(\mathbf{f}_{mk}^{\mathtt{dl}}\right)^{\mathrm{H}}\mathbf{v}_{mk'}^{\mathtt{dl}}s_{k'}^{\mathtt{dl}} + \sum\nolimits_{l\in\mathcal{L}} h_{k\ell}x_\ell^{\mathtt{ul}} + w_k^{\mathtt{dl}}, \quad (26)$$

where ρ_d denotes the normalized DL SNR, a_m denotes the binary AP mode assignment variable with $a_m = 1$ indicating that AP m operates in the DL mode; μ_{mk} denotes the power control coefficient at AP m corresponding to $\mathrm{U}_k^{\mathtt{dl}}$, $\mathbf{v}_{mk}^{\mathtt{dl}} \in \mathbb{C}^{N\times 1}$ is the precoding vector at AP m for DL UE k, $s_k^{\mathtt{dl}} \sim \mathcal{CN}(0,1)$ denotes the intended symbol for $\mathrm{U}_k^{\mathtt{dl}}$, while $w_k^{\mathtt{dl}} \sim \mathcal{CN}(0,1)$ is the AWGN at DL UE k. Note that the third term in (26) is the cross-link interference (CLI) caused by the UL UEs due to concurrent transmissions of DL and UL UEs over the same frequency band, while $x_\ell^{\mathtt{ul}}$ denotes the transmit signal from the $\mathrm{U}_l^{\mathtt{ul}}$. We assume that AP m uses the available CSI to locally form the MRT precoding vector for DL UE $k \in \mathcal{W}_m^{\mathtt{dl}}$ as $\mathbf{v}_{mk}^{\mathtt{dl,MR}} = \hat{\mathbf{f}}_{mk}^{\mathtt{dl}}$.

With MRT precoding, the achievable DL SE at the k-th DL UE is given by

$$\mathcal{S}_k^{\mathtt{dl}}(\mathbf{a},\boldsymbol{\mu},\boldsymbol{\varsigma}) = \frac{\tau_c-\tau_p}{\tau_c}\log_2\left(1+\frac{\rho_d(\sum_{m\in\mathcal{M}} N a_m\mu_{mk}\gamma_{mk}^{\mathtt{dl}})^2}{\Omega_k(\boldsymbol{\mu},\boldsymbol{\varsigma},\mathbf{a})}\right), \quad (27)$$

where

$$\Omega_k(\boldsymbol{\mu},\boldsymbol{\varsigma},\mathbf{a}) = \rho_d\sum\nolimits_{m\in\mathcal{M}}\sum\nolimits_{k'\in\mathcal{K}} N a_m\mu_{mk'}^2\gamma_{mk'}^{\mathtt{dl}}\zeta_{f_{mk}}^{\mathtt{dl}} + \rho_u\sum\nolimits_{l\in\mathcal{L}}\tilde{\varsigma}_l\zeta_{h_{kl}}^{\mathtt{du}} + 1. \quad (28)$$

Moreover, $\mathbf{a} \triangleq \{a_m\}$; $\boldsymbol{\mu} \triangleq \{\mu_{mk}\}$ denote the DL power control coefficients at AP $m \in \mathcal{M}$ towards $\mathrm{U}_k^{\mathtt{dl}}$, $\forall k \in \mathcal{K}$; $\boldsymbol{\varsigma} \triangleq \{\varsigma_l\}$, present the UL power control coefficients for $\mathrm{U}_l^{\mathtt{ul}}$, $\forall l \in \mathcal{L}$; ρ_u denotes the normalized UL SNR; $\gamma_{mk}^{\mathtt{dl}}$ is the variance of the MMSE estimate of $\mathbf{f}_{mk}^{\mathtt{dl}}$, i.e., $\hat{\mathbf{f}}_{mk}^{\mathtt{dl}} \sim \mathcal{CN}(\mathbf{0}, \gamma_{mk}^{\mathtt{dl}}\mathbf{I}_N)$.

UL Data Transmission: The transmit signal from UL UE ℓ is represented by $x_\ell^{\mathtt{ul}} = \sqrt{\rho_u \varsigma_\ell} s_\ell^{\mathtt{ul}}$, where $s_\ell^{\mathtt{ul}}$ (with $\mathbb{E}\left\{|s_\ell^{\mathtt{ul}}|^2\right\} = 1$) and ρ_u denote the transmitted symbol by $\mathrm{U}_l^{\mathtt{ul}}$ and the normalized transmit power at each UL UE, while ς_ℓ is the transmit power control coefficient at $\mathrm{U}_l^{\mathtt{ul}}$ with $0 \leq \varsigma_\ell \leq 1, \forall \ell$.

The received signal $\mathbf{y}_m^{\mathtt{ul}} \in \mathbb{C}^{N\times 1}$ at AP m in the UL mode can be written as

$$\begin{aligned}\mathbf{y}_m^{\mathtt{ul}} &= \sqrt{\rho_u} \sum\nolimits_{l\in\mathcal{L}} \sqrt{b_m \tilde{\varsigma}_l} \mathbf{g}_{ml}^{\mathtt{ul}} s_l^{\mathtt{ul}} \\ &+ \underbrace{\sqrt{\rho_d} \sum\nolimits_{i\in\mathcal{M}\setminus m} \sum\nolimits_{k\in\mathcal{K}} \sqrt{b_m a_i} \mu_{ik} \mathbf{Q}_{mi} \mathbf{v}_{ik}^{\mathtt{dl}} s_k^{\mathtt{dl}}}_{\text{Intra-AP interference}} \\ &+ \underbrace{\sqrt{\rho_d} \sum\nolimits_{k\in\mathcal{K}} \sqrt{b_m a_m} \mu_{mk} \mathbf{Q}_{mm} \mathbf{v}_{mk}^{\mathtt{dl}} s_k^{\mathtt{dl}}}_{\text{Inter-AP (SI) interference}} + \sqrt{b_m} \mathbf{w}_m^{\mathtt{ul}},\end{aligned} \tag{29}$$

where b_m denotes the binary AP mode assignment variable with $b_m = 1$ indicating that AP m operates in the UL mode and $\mathbf{w}_m^{\mathtt{ul}}$ is the AWGN vector with $\mathcal{CN}(0,1)$ distributed elements. In (29), the second term captures the interference from APs transmitting towards DL UEs, and the third term represents the SI term wherever AP m is FD-enabled (i.e., $b_m a_m = 1$).

In order to improve the achievable UL SE, the signals forwarded to the CPU from the UL APs m, corresponding to UE l, are further multiplied by the LSFD weight α_{ml}, $\forall m, l$. The aggregated received signal for UL UE $\ell, \forall \ell$ with $|\alpha_{ml}|^2 \leq 1, \forall \ell, m$ at the CPU can be written as

$$\mathbf{r}_\ell^{\mathtt{ul}} = \sum\nolimits_{m\in\mathcal{M}} \alpha_{ml} (\mathbf{v}_{m\ell}^{\mathtt{ul}})^{\mathrm{H}} \mathbf{y}_m^{\mathtt{ul}}. \tag{30}$$

Finally, $s_\ell^{\mathtt{ul}}$ is detected from $\mathbf{r}_\ell^{\mathtt{ul}}$.

We assume that MRC is performed at the IBFD/UL HD AP with $\mathbf{v}_{m\ell}^{\mathtt{ul,MR}} = \hat{\mathbf{g}}_{ml}^{\mathtt{ul}}$ and data is transferred to the CPU for UL data reception. The achievable UL SE for the l-th UL UE at the CPU is given by

$$\mathcal{S}_l^{\mathtt{ul}}(\mathbf{a},\mathbf{b},\boldsymbol{\varsigma},\boldsymbol{\mu},\boldsymbol{\alpha}) = \frac{\tau_c - \tau_p}{\tau_c} \log_2(1 + \mathtt{SINR}_l^{\mathtt{ul}}(\mathbf{a},\mathbf{b},\boldsymbol{\varsigma},\boldsymbol{\mu},\boldsymbol{\alpha})), \tag{31}$$

where $\mathbf{b} \triangleq \{b_m\}$ and

$$\mathtt{SINR}_l^{\mathtt{ul}}(\mathbf{b},\boldsymbol{\varsigma},\boldsymbol{\mu},\boldsymbol{\alpha}) = \frac{\rho_u \left(\sum_{m\in\mathcal{M}} N\alpha_{ml}\sqrt{b_m\varsigma_l}\gamma_{ml}^{\mathtt{ul}}\right)^2}{\Phi_l(\mathbf{b},\boldsymbol{\varsigma},\boldsymbol{\mu},\boldsymbol{\alpha}) + \rho_d \sum_{i\in\mathcal{M}} \sum_{q\in\mathcal{K}} a_i \mu_{iq}^2 \gamma_{iq}^{\mathtt{dl}} \Psi_{li}(\mathbf{b},\boldsymbol{\alpha})}, \tag{32}$$

where $\gamma_{ml}^{\mathtt{ul}}$ is the variance of the MMSE estimate of $\mathbf{g}_{ml}^{\mathtt{ul}}$ and

$$\begin{aligned}\Phi_l(\mathbf{b},\boldsymbol{\varsigma},\boldsymbol{\mu},\boldsymbol{\alpha}) &= \rho_u \sum\nolimits_{m\in\mathcal{M}} \sum\nolimits_{l'\in\mathcal{L}} \Big(N\alpha_{ml}^2 b_m \varsigma_{l'} \gamma_{ml}^{\mathtt{ul}} \zeta_{g_{ml'}}^{\mathtt{ul}} \\ &\quad + N\alpha_{ml}^2 b_m \gamma_{ml}^{\mathtt{ul}}\Big), \end{aligned} \tag{33a}$$

$$\Psi_{li}(\mathbf{b},\boldsymbol{\alpha}) = \sum\nolimits_{m\in\mathcal{M}} N^2 \alpha_{ml}^2 b_m \gamma_{ml}^{\mathtt{ul}} \zeta_{Q_{mi}}. \tag{33b}$$

Power consumption: Let P_ℓ and $P_{\mathrm{U},\ell}$ be the power consumption for transmitting signals and the required power consumption to run the circuit components for the UL transmission at $\mathrm{U}_l^{\mathtt{ul}}$. Moreover, assume that $P_{\mathrm{D},k}$ denotes the power consumption to run the circuit components for the DL transmission at $\mathrm{U}_k^{\mathtt{dl}}$; $P_{\mathtt{bh},m}$ is the power consumed by the fronthaul link between the CPU and AP m. Therefore, the total power consumption over the considered CF NAFD system is modeled as [120], [141]

$$\begin{aligned}P_{\mathtt{total}} &= \sum\nolimits_{\ell\in\mathcal{L}} (P_\ell + P_{\mathrm{U},\ell}) + \sum\nolimits_{m\in\mathcal{M}} P_m \\ &\quad + \sum\nolimits_{k\in\mathcal{K}} P_{\mathrm{D},k} + \sum\nolimits_{m\in\mathcal{M}} P_{\mathtt{bh},m},\end{aligned} \tag{34}$$

where P_m denotes the power consumption at AP m that includes the power consumption of the transceiver chains and the power consumed for the DL or UL transmission. The power consumption P_m can be modeled as [130]

$$\begin{aligned}P_m(\boldsymbol{a},\boldsymbol{b},\boldsymbol{\theta}) &= \frac{1}{\zeta_m}\rho_d\sigma_n^2 \left(N \sum\nolimits_{k\in\mathcal{K}} \gamma_{mk}^{\mathtt{dl}} \mu_{mk}\right) + a_m N P_{\mathtt{cdl},m} \\ &\quad + b_m N P_{\mathtt{cul},m},\end{aligned} \tag{35}$$

where $0 < \zeta_m \leq 1$ is the power amplifier efficiency at the m-th AP, σ_n^2 is the noise power; $P_{\mathtt{cdl},m}$ and $P_{\mathtt{cul},m}$ is the internal power required to run the circuit components (e.g., converters, mixers, and filters) related to each antenna of AP m for the DL and UL transmissions, respectively. The power consumption at $\mathrm{U}_l^{\mathtt{ul}}$ is given by

$$P_\ell = \frac{1}{\chi}\rho_u \sigma_n^2 \varsigma_\ell, \tag{36}$$

where χ is the power amplifier efficiency at UL UEs.

The power consumption of the fronthaul signal load to each AP m is proportional to the fronthaul rate as [120]

$$P_{\mathtt{bh},m} = a_m P_{\mathtt{fdl},m} + b_m P_{\mathtt{ful},m} + R_m P_{\mathtt{bt},m}, \tag{37}$$

where $P_{\mathtt{bt},m}$ is the traffic-dependent fronthaul power (in Watt per bit/s) and R_m is the fronthaul rate between AP m and the CPU, given by

$$\begin{aligned}R_m = B\Big(&a_m \sum\nolimits_{\ell\in\mathcal{L}} \mathcal{S}_\ell^{\mathtt{ul}}(\mathbf{b},\boldsymbol{\varsigma},\boldsymbol{\mu},\boldsymbol{\alpha}) \\ &+ b_m \sum\nolimits_{k\in\mathcal{K}} \mathcal{S}_k^{\mathtt{dl}}(\mathbf{a},\boldsymbol{\mu},\boldsymbol{\varsigma})\Big).\end{aligned} \tag{38}$$

By substituting (35), (36), and (37) into (34), we have

$$\begin{aligned}P_{\mathtt{total}}(\mathbf{a},\mathbf{b},\boldsymbol{\varsigma},\boldsymbol{\mu},\boldsymbol{\alpha}) &= \sum_{m\in\mathcal{M}} \frac{N\rho_d\sigma_n^2}{\zeta_m} \left(\sum\nolimits_{k\in\mathcal{K}} \gamma_{mk}^{\mathtt{dl}} \mu_{mk}\right) \\ &\quad + \sum\nolimits_{\ell\in\mathcal{L}} \frac{\rho_u\sigma_n^2}{\chi}\varsigma_\ell + P_{\mathrm{U},\mathtt{fixed}} + R_m P_{\mathtt{bt},m} \\ &\quad + \sum\nolimits_{m\in\mathcal{M}} a_m (N P_{\mathtt{cdl},m} + P_{\mathtt{fdl},m}) \\ &\quad + \sum\nolimits_{m\in\mathcal{M}} b_m (N P_{\mathtt{cul},m} + P_{\mathtt{ful},m}),\end{aligned} \tag{39}$$

where $P_{\mathrm{U},\mathtt{fixed}} \triangleq \sum_{k\in\mathcal{L}} P_{\mathrm{U},\ell} + \sum_{k\in\mathcal{K}} P_{\mathrm{D},k}$.

System design: The AP mode assignment problem involves determining the UL and DL mode assignment vectors $(\mathbf{a},\mathbf{b})$, the power control coefficients $(\boldsymbol{\varsigma},\boldsymbol{\mu})$, and the LSFD weight vector $\boldsymbol{\alpha}$. The objective is to maximize the EE of the CF NAFD while adhering to constraints on the per-user SE, the

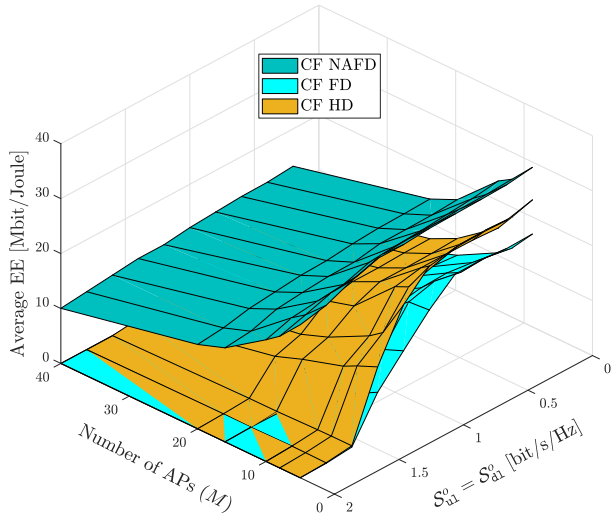

Fig. 10: Average EE versus $\mathcal{S}^o_{\mathtt{dl}} = \mathcal{S}^o_{\mathtt{ul}}$ for different values of M ($MN = 80$, $K = L = 4$, $\tilde{\rho}_u = 0.2$ Watt, $\tilde{\rho}_d = 1$ Watt, $\sigma^2_{\mathtt{SI},m}/\sigma^2_n = 50$ dB, $B = 50$ MHz).

transmit power at each AP, and the UL UE. More precisely, the optimization problem is formulated as

$$\mathbf{P2}: \max_{\mathbf{a},\mathbf{b},\boldsymbol{\varsigma},\boldsymbol{\mu},\boldsymbol{\alpha}} \quad \mathtt{EE} \triangleq \frac{R_m(\mathbf{a},\mathbf{b},\boldsymbol{\varsigma},\boldsymbol{\mu},\boldsymbol{\alpha})}{P_{\mathtt{total}}(\mathbf{a},\mathbf{b},\boldsymbol{\varsigma},\boldsymbol{\mu},\boldsymbol{\alpha})} \tag{40a}$$

$$\text{s.t} \quad \mathcal{S}^{\mathtt{ul}}_{\ell}(\mathbf{b},\boldsymbol{\varsigma},\boldsymbol{\mu},\boldsymbol{\alpha}) \geq \mathcal{S}^o_{\mathtt{ul}}, \ \forall \ell, \tag{40b}$$

$$\mathcal{S}^{\mathtt{dl}}_{k}(\mathbf{a},\boldsymbol{\mu},\boldsymbol{\varsigma}) \geq \mathcal{S}^o_{\mathtt{dl}}, \ \forall k, \tag{40c}$$

$$\sum\nolimits_{k\in\mathcal{K}} N\gamma^{\mathtt{dl}}_{mk}\theta^2_{mk} \leq a_m, \tag{40d}$$

$$|\alpha_{ml}|^2 \leq 1, \forall \ell, m, \tag{40e}$$

$$a_m, b_m \in \{0,1\}, \tag{40f}$$

$$0 \leq \varsigma_\ell \leq 1, \forall \ell, \tag{40g}$$

where $\mathcal{S}^o_{\mathtt{ul}}$ and $\mathcal{S}^o_{\mathtt{dl}}$ are the minimum SEs required by the $\mathrm{U}^{\mathtt{ul}}_l$ and $\mathrm{U}^{\mathtt{dl}}_k$, respectively, to guarantee the QoS in the network. Moreover, constraint (40d) is the per-AP transmit power constraint.

Figure 10 compares the average EE performance of CF NAFD and conventional CF system designs as a function of $\mathcal{S}^o_{\mathtt{dl}} = \mathcal{S}^o_{\mathtt{ul}}$ and M, with the number of service antennas kept fixed at $MN = 40$. The path-loss model from [142] has been considered, and the parameters of the power consumption are set according to [130, Table II]. It can be observed that NAFD satisfactorily supports the SE requirements of both UL and DL UEs, while both the FD and HD setups fail to meet SE requirements greater than 1.2 [bit/s/Hz].

VI. Challenges and Future Research Directions

This section addresses open challenges, trends, and the potential use of CF FD with other wireless technologies.

A. mmWave Communications

With its wide frequency spectrum (30–100 GHz), mmWave communication offers significantly higher capacity than current WLANs and cellular systems, making it a key technology for next-generation wireless networks [143]–[145]. However, mmWave signals face extremely high path loss due to foliage, atmospheric absorption, rain fading, and obstacle sensitivity, which lowers the received SINR. To compensate and achieve a sufficient link budget, dense antenna arrays with joint transmit-receiver beamforming are needed to provide substantial directional gains. Fortunately, the small mmWave wavelength allows large antenna arrays to be packed into compact devices. Additionally, unlike omnidirectional transmissions that create widespread interference, directional transmissions inherently limit interference to fewer nodes.

Nevertheless, recent advances in mmWave communication — including digital/analog beamforming with dense antenna arrays and fewer RF chains — now enable mmWave FD communication by overcoming significant path loss and achieving sufficient link margin [146]–[148]. While conventional sub-6 GHz FD techniques cannot be directly applied due to fundamental differences (e.g., propagation characteristics, hybrid beamforming, wide bandwidths, high sampling rates, and beam alignment), novel transmission strategies have been developed to explore the feasibility of mmWave FD systems [146]–[152].

However, traditional cell-based mmWave FD systems cannot meet the growing communication demands [153]. Integrating mmWave with CF FD technology offers a promising path for next-generation wireless networks. The macro-diversity gains from distributed APs help overcome mmWave's limited coverage, while flexible duplex modes and efficient bidirectional communication are enabled through CLI cancellation [101]. Additionally, hybrid analog-digital beamforming can offset the significant free-space path loss at higher frequencies [153], making this integration a key enabler for advancing next-generation wireless capabilities.

Few studies have explored the viability of mmWave CF FD communication [154], [155]. Reference [154] examined a mmWave CF NAFD system, proposing cooperative resource allocation and beamforming with location-aided channel estimation to minimize inter-user interference. Specifically, it leveraged LoS-dominated channels by reconstructing inter-user channels from user locations, enabling joint AP mode selection and beamforming. Reference [155] investigated a mmWave CF NAFD system with DAC quantization and fronthaul compression, focusing on weighted UL and DL sum rate maximization through joint optimization of remote antenna transmit power, UL user power, and fronthaul compression noise variance.

B. UAV Communications

UAVs, also known as drones, have caught the attention of the research community recently due to their autonomy, flexibility, and wide range of applications, including military, surveillance and monitoring, telecommunications, medical supply delivery, rescue operations, and more [156]–[159]. Although traditional UAV-centric research focuses on enhancing control and autonomy due to robotics or military applications, UAV-assisted communications, i.e., flying BSs or mobile relays, have recently emerged [156]–[159]. In such

cases, UAVs serve as aerial communication platforms, providing/improving communication services to ground targets in high traffic demand and overloaded situations. Due to the high altitude of UAVs, there is a greater likelihood of LoS links between the ground UEs and APs, resulting in improved channel quality compared to terrestrial networks.

Recent UAV research has focused on integrating FD transceivers in UAV networks [158]–[165] and CF UAV communication [166]–[172] to improve the SE. While these approaches have been studied separately, combining UAVs with CF FD technology presents a promising yet unexplored research direction for enhancing UAV network performance. However, FD communication in low-altitude 3-D coverage scenarios is challenging due to increased UL and DL traffic and amplified interference from LoS links. Recent works [173]–[175] have introduced the NAFD concept into aerial-ground CF systems to achieve flexible duplex communication in the spatial domain, allowing UAVs to select duplex modes based on the traffic distribution.

C. Reconfigurable Intelligent Surfaces

RISs, or intelligent reflecting surfaces, provide cost-effective, energy-efficient, and spectrum-efficient communications [176]–[179]. An RIS comprises a planar array of hundreds or thousands of "nearly passive" reflecting elements. A software controller can control the reflective properties of these components individually, changing the real-time response to dynamic wireless channels, abrupt network changes, and/or traffic demands. In particular, the controller can customize the individual elements to change their states to achieve coherent combining for the reflected signals at chosen receivers, thus increasing the received signal power. At the same time, the reflected signals combine destructively at non-intended receivers, suppressing co-channel interference or increasing the secrecy rate [176], [177]. Furthermore, since no transmit RF chains or amplifiers are required, an RIS panel may consume only a few Watts of power during the reconfiguration stages and significantly less during idle states. For 3-, 4-, 5-, and 6-bit resolution phase shifting, typical power consumption values per each phase shifter are respectively 1.5, 4.5, 6, and 7.8 mW [180]. Even without an amplifier, an RIS may produce significant gain—about 30 to 40 decibels relative to isotropic (dBi) depending on surface size and frequency [181]. As a result, an RIS has much lower hardware/energy cost than standard active antenna arrays [168], [176], [182].

An RIS resembles an FD device without antenna noise amplification or SI, providing an efficient alternative for FD relays needing complicated SIC methods. Although the integration of FD with RISs is being actively researched in traditional co-located MIMO setups [183]–[186], only a limited amount of work exists in HD CF systems [187]–[189] whilst the first papers on the CF FD with RIS are yet to appear.

With the current investigations on RIS in many wireless systems, such as HD CF, mMIMO, IoT, and many others [183]–[186], it can be anticipated that they will present significant advantages and opportunities for CF FD systems. By dynamically adjusting the phase and amplitude of reflected signals, an RIS can enhance the signal strength, improve coverage, and facilitate better interference management. This capability is crucial for mitigating the SI inherent in FD operations. Furthermore, an RIS can bolster security by creating dynamic, adaptive signal paths that are harder for eavesdroppers to intercept. The improved SE and energy savings resulting from optimized signal reflections would also contribute to more robust and efficient CF FD networks.

D. Integrated Sensing and Communications

Among many visionary considerations about 6G wireless networks, a common theme is that sensing will play a more significant role than ever before. It is anticipated that future wireless networks will be able to image and measure the surrounding environment, thereby enabling advanced location-aware services. This synergy between communication and sensing is referred to as ISAC and finds applications in various emerging areas, including vehicular networks, environmental monitoring, and human activity recognition. Recently, ISAC has garnered recognition from the International Telecommunication Union (ITU) as a pivotal element within the 6G landscape, serving as one of six key 6G usage scenarios [190].

ISAC can be realized through a synergistic design of communications and radar/sensing systems that share spectral and hardware resources [191], [192]. This involves developing strategies for cohabitation designs and/or dynamic spectrum allocation and access, along with interference suppression or management [191], [192]. Alternatively, ISAC can be implemented from a co-design perspective, allowing communications and radar/sensing systems to operate in parallel with jointly optimized performance [193]–[197]. Therefore, ISAC offers two primary advantages over dedicated sensing and communication functionalities. Firstly, it provides integration gains, enabling the efficient utilization of congested resources. Secondly, it offers coordination gains, allowing for the balancing of multi-functional performance and mutual assistance. The rapid evolution of ISAC suggests a future dual-functional network that could enable innovative services for civilians. In this network, the sensing operation collects and extracts information from noisy observations, while communication transfers information through specifically tailored signals and recovers it [193]–[197].

ISAC has primarily been studied in single-cell scenarios with monostatic sensing, where the transmitter and receiver are co-located for sensing [198]–[201]. However, distributed designs can be employed to leverage macro diversity gain, thereby mitigating the effects of large-scale fading in single-cell scenarios. In line with this, the integration of CF and ISAC has been explored in a few recent studies [202]–[204]. The systems considered in these studies operate in a multi-static manner [194], i.e., multiple non-co-located transmitters and receivers are deployed. Specifically, the design in [202] assumed that all the APs serve the UEs over the same time-frequency resources, while the sensing signal for a specific target is generated by its designated AP (only some specific APs serve as an ISAC transmitter). The echo signals reflected by the target are received by all APs and sent back to the CPU

for further processing (all APs serve as ISAC receivers). Consequently, the APs operate in FD mode to receive the reflected signals. However, from the sensing perspective, the main focus of this study is beampattern design at the transmitter, and the challenges related to the FD operation at the APs during the reception of echo signals remain unexplored. In [203], an ISAC system with DL communication and multi-static sensing in a cloud radio access network (C-RAN) architecture has been considered, wherein each AP either serves as an ISAC transmitter or a sensing receiver. This architecture dispenses with the FD capability requirement in monostatic sensing while stimulating FD operation via HD APs and reflecting the use of the NAFD concept for ISAC CF systems. However, the operation mode of the APs is fixed. A more flexible design has been proposed in [204], where, depending on the network requirements, the operation mode of the APs is determined as either a communication or sensing AP. Inter-system interference is managed through joint operation mode selection and power control design at the APs.

E. Machine Learning

ML transforms wireless networks by enhancing the signal processing, network management, spectrum utilization, and security. By leveraging data-driven insights, ML improves the performance and reliability while addressing the growing complexity of modern wireless systems and underpinning advanced technologies.

ML has thus been widely applied in CF networks across various tasks, including channel estimation [205], power control [206], beamforming design [207], [208], and UE clustering in NOMA CF systems [207]. These studies leverage ML to address the high-dimensional and nonlinear optimization challenges inherent in CF networks. ML algorithms can process large datasets in real time, which is well-suited for large-scale deployments, effectively addressing scalability issues. Moreover, ML facilitates real-time decision-making for resource management, performance optimization, and low-latency communication. The introduction of AP mode selection in CF NAFD networks further increases the complexity of optimization, where ML offers promising solutions [132], [173], [175].

F. Tailored SIC Techniques for CF FD

The FD operation in CF mMIMO presents unique opportunities to enhance the network performance. Unlike co-located FD systems, CF FD systems avail of the proximity between APs and users, which allows for lower transmit power levels at APs. This inherently reduces the impact of SI. Recent research has explored various SI mitigation techniques for CF FD networks. For instance, reference [100] demonstrated that power control can effectively mitigate the residual SI by leveraging a large number of distributed APs. In [102], passive SI suppression was achieved by exploiting the path loss and strategically allocating the transmit and receive antennas at different APs. Additionally, [49] highlighted that when APs are equipped with multiple antennas, spatial processing techniques, such as null-space projection and beamforming, can further suppress SI.

These studies illustrate that spatial signal processing plays a crucial role in SI mitigation. However, most existing CF FD research still relies on conventional SIC techniques originally developed for co-located FD systems. Applying these techniques directly to CF FD networks introduces several challenges. First, equipping each distributed AP with dedicated SI suppression hardware, such as directional isolation, antenna separation, and adaptive filtering, can be costly and impractical for large-scale deployments. Second, the characteristics of the SI channel in distributed networks differ significantly from those in co-located systems, as the spatial distribution of APs influences the SI propagation and correlation. For example, [209] showed that SIC performance in multi-antenna systems is highly dependent on the SI channel modeling and beamforming design. Similar considerations must be made for CF FD systems to ensure effective SI mitigation across multiple distributed APs.

Moreover, beamforming strategies in CF FD networks require careful design to suppress the SI while minimizing inter-AP and co-channel interference. Unlike co-located FD systems, where centralized beamforming optimization is feasible, CF FD networks require distributed or hierarchical beamforming approaches to balance SI suppression and inter-user interference management. Advanced spatial processing techniques, such as eigenmode transmission and adaptive null-space projection, must be adapted to the distributed nature of CF FD networks. While current CF FD research primarily relies on existing SIC strategies, future research should focus on developing scalable, low-overhead SI mitigation techniques specifically designed for massive CF FD deployments. These advancements will be crucial to fully harness the potential of CF FD networks in next-generation wireless systems.

G. Large-Scale CF FD Networks

Deploying CF FD in large-scale networks with numerous wireless devices, including communication, sensing, and computing-oriented users, introduces several challenges. These include the additional overhead required for CSI acquisition, signal processing, and coordination among distributed APs. Moreover, the interplay between distributed FD operation, SI, and inter-user interference significantly impacts the system performance and overhead requirements.

To address these challenges, advanced and scalable CSI acquisition techniques, such as ML, deep learning-based estimation, and tensor-based compressed sensing [205], can significantly reduce the overhead by leveraging temporal and spatial correlations to enhance CSI accuracy with minimal feedback. Intelligent AP selection, where only a subset of APs actively serve users based on channel conditions, further lowers signaling and computational costs while maintaining system performance [6]. Moreover, not all APs need to operate in FD mode continuously; dynamic AP assignment, i.e., hybrid FD/HD operation, allows APs to switch between modes based on interference, network load, and SI levels, as seen in CF NAFD networks [44], [101]. This hybrid approach effectively

balances the performance gains of FD operation with the complexity of SIC.

To further mitigate the signaling overhead, grant-free transmission schemes, where users transmit without explicit scheduling, can be integrated with CF FD systems [210], [211]. Combined with advanced interference management techniques, this can improve scalability and efficiency in massive-device scenarios [210], [211]. Moreover, the centralized CPU-based processing in conventional CF systems may not scale well for large-scale CF FD due to the increased overhead of handling SI and FD interference. Edge-based or hierarchical distributed processing architectures can reduce signaling overhead and improve network performance [212], [213]. On the other hand, given the increasing importance of sensing-oriented users in future networks, CF FD systems can be adapted to jointly optimize communication and sensing objectives. For instance, the FD APs can be repurposed for environment-aware sensing rather than purely being assigned for communication [201], [214]. This dual-functional use of FD operation can enhance the network utility without additional signaling costs.

H. Unexplored Research Avenues

Aside from the above-mentioned research directions, the integration of CF FD with other well-known technologies, including backscatter communications, mobile edge computing, rate splitting multiple access, vehicle-to-everything communication, underwater wireless communication, age of information, and more, remains untouched as of today.

VII. Conclusion

This research investigated the potential and advantages of CF FD systems for the next generation of wireless networks. Initially, the fundamentals of FD communication and CF architecture were reviewed, highlighting their impact on current wireless systems. The integration of FD technology into CF architectures was then examined, focusing on channel estimation, performance analysis, and resource allocation. CF NAFD networks were also explored, supported by a comprehensive literature survey and case studies using a general CF FD system configuration. Additionally, emerging CF FD paradigms, such as mmWave communications, UAV communication, RIS, ISAC, and others, were discussed. Finally, several research gaps were identified, providing a foundation for future research efforts.

References

[1] Samsung, "White paper: The vision of 6G bring the next hyper-connected experience to every corner of life," Jul. 2020. Available Online: https://research.samsung.com/next-generation-communications.

[2] M. Matthaiou *et al.*, "The road to 6G: Ten physical layer challenges for communications engineers," *IEEE Commun. Mag.*, vol. 59, no. 1, pp. 64–69, Jan. 2021.

[3] H. He, X. Yu, J. Zhang, S. H. Song, and K. B. Letaief, "Cell-free massive MIMO for 6G wireless communication networks," *J. Commun. Inf. Netw.*, vol. 6, no. 4, pp. 321–335, Nov. 2021.

[4] J. Zhang, S. Chen, Y. Lin, J. Zheng, B. Ai, and L. Hanzo, "Cell-free massive MIMO: A new next-generation paradigm," *IEEE Access*, vol. 7, pp. 99 878–99 888, Aug. 2019.

[5] H. Q. Ngo, A. Ashikhmin, H. Yang, E. G. Larsson, and T. L. Marzetta, "Cell-free massive MIMO versus small cells," *IEEE Trans. Wireless Commun.*, vol. 16, no. 3, pp. 1834–1850, Mar. 2017.

[6] E. Björnson and L. Sanguinetti, "Scalable cell-free massive MIMO systems," *IEEE Trans. Commun.*, vol. 68, no. 7, pp. 4247–4261, Jul. 2020.

[7] H. Q. Ngo, G. Interdonato, E. G. Larsson, G. Caire, and J. G. Andrews, "Ultradense cell-free massive MIMO for 6G: Technical overview and open questions," *Proc. IEEE*, vol. 112, no. 7, pp. 805–831, Jul. 2024.

[8] Ö. Demir, E. Björnson, and L. Sanguinetti, *Foundations of User-Centric Cell-Free Massive MIMO*, ser. Foundations and trends in signal processing. Now Publishers, 2021.

[9] T. Riihonen, S. Werner, and R. Wichman, "Hybrid full-duplex/half-duplex relaying with transmit power adaptation," *IEEE Trans. Wireless Commun.*, vol. 10, no. 5, pp. 3074–3085, Sept. 2011.

[10] M. Duarte, C. Dick, and A. Sabharwal, "Experiment-driven characterization of full-duplex wireless systems," *IEEE Trans. Wireless Commun.*, vol. 11, no. 12, pp. 4296–4307, Dec. 2012.

[11] E. Everett, A. Sahai, and A. Sabharwal, "Passive self-interference suppression for full-duplex infrastructure nodes," *IEEE Trans. Wireless Commun.*, vol. 13, no. 2, pp. 680–694, Feb. 2014.

[12] S. Hong *et al.*, "Applications of self-interference cancellation in 5G and beyond," *IEEE Commun. Mag.*, vol. 52, no. 2, pp. 114–121, Feb. 2014.

[13] J. I. Choi, M. Jain, K. Srinivasan, P. Levis, and S. Katti, "Achieving single channel, full duplex wireless communication," in *Proc. ACM MobiCom*, Sept. 2010, p. 1–12.

[14] E. Everett, M. Duarte, C. Dick, and A. Sabharwal, "Empowering full-duplex wireless communication by exploiting directional diversity," in *Proc. IEEE Asilomar CSSC*, Nov. 2011, pp. 2002–2006.

[15] B. Radunovic *et al.*, "Rethinking indoor wireless mesh design: Low power, low frequency, full-duplex," in *Proc. IEEE WiMesh*, Jun. 2010, pp. 1–6.

[16] W. Cheng, X. Zhang, and H. Zhang, "Full/half duplex based resource allocations for statistical quality of service provisioning in wireless relay networks," in *Proc. IEEE INFOCOM*, Mar. 2012, pp. 864–872.

[17] T. Riihonen, S. Werner, and R. Wichman, "Comparison of full-duplex and half-duplex modes with a fixed amplify-and-forward relay," in *Proc. IEEE WCNC*, Apr. 2009, pp. 1–5.

[18] B. Chun and Y. H. Lee, "A spatial self-interference nullification method for full duplex amplify-and-forward MIMO relays," in *Proc. IEEE WCNC*, Apr. 2010, pp. 1–6.

[19] G. Liu, F. R. Yu, H. Ji, V. C. M. Leung, and X. Li, "In-band full-duplex relaying: A survey, research issues and challenges," *IEEE Commun. Surveys Tuts.*, vol. 17, no. 2, pp. 500–524, Secondquarter 2015.

[20] D. Kim, H. Lee, and D. Hong, "A survey of in-band full-duplex transmission: From the perspective of PHY and MAC layers," *IEEE Commun. Surveys Tuts.*, vol. 17, no. 4, pp. 2017–2046, Fourthquarter 2015.

[21] A. Balatsoukas-Stimming, "Non-linear digital self-interference cancellation for in-band full-duplex radios using neural networks," in *Proc. IEEE SPAWC*, Jun. 2018, pp. 1–5.

[22] H. Guo, S. Wu, H. Wang, and M. Daneshmand, "DSIC: Deep learning based self-interference cancellation for in-band full duplex wireless," in *Proc. IEEE GLOBECOM*, Dec. 2019, pp. 1–6.

[23] A. T. Kristensen, A. Burg, and A. Balatsoukas-Stimming, "Advanced machine learning techniques for self-interference cancellation in full-duplex radios," in *Proc. IEEE Asilomar CSSC*, Nov. 2019, pp. 1149–1153.

[24] A. Balatsoukas-Stimming, *Neural Networks for Full-Duplex Radios*. John Wiley & Sons, Ltd, 2020, ch. 18, pp. 383–396.

[25] V. Tapio and M. Juntti, "Non-linear self-interference cancelation for full-duplex transceivers based on Hammerstein-Wiener model," *IEEE Commun. Lett.*, vol. 25, no. 11, pp. 3684–3688, Nov. 2021.

[26] V. Panse, T. K. Jain, P. K. Sharma, and A. Kothari, "Digital self-interference cancellation in the era of machine learning: A comprehensive review," *Physical Commun.*, vol. 50, p. 101526, Feb. 2022.

[27] K. E. Kolodziej, A. U. Cookson, and B. T. Perry, "RF canceller tuning acceleration using neural network machine learning for in-band full-duplex systems," *IEEE Open J. Commun. Soc.*, vol. 2, pp. 1158–1170, May 2021.

[28] ——, "Neural network tuning for analog-RF self-interference cancellation," in *Proc. IEEE MTT-S Int. Microw. Symposium*, Jun. 2021, pp. 673–676.

[29] H. A. Ammar, R. Adve, S. Shahbazpanahi, G. Boudreau, and K. V. Srinivas, "User-centric cell-free massive MIMO networks: A survey of

opportunities, challenges and solutions," *IEEE Commun. Surveys Tuts.*, vol. 24, no. 1, pp. 611–652, Firstquarter 2022.

[30] G. Interdonato, E. Björnson, H. Q. Ngo, P. K. Frenger, and E. G. Larsson, "Ubiquitous cell-free massive MIMO communications," *EURASIP J. Wireless Commun. Netw.*, vol. 2019, pp. 1687–1499, Aug. 2019.

[31] J. Zhang, E. Björnson, M. Matthaiou, D. W. K. Ng, H. Yang, and D. J. Love, "Prospective multiple antenna technologies for beyond 5G," *IEEE J. Sel. Areas Commun.*, vol. 38, no. 8, pp. 1637–1660, Aug. 2020.

[32] S. Elhoushy, M. Ibrahim, and W. Hamouda, "Cell-free massive MIMO: A survey," *IEEE Commun. Surveys Tuts.*, vol. 24, no. 1, pp. 492–523, Firstquarter 2022.

[33] S. Chen, J. Zhang, J. Zhang, E. Björnson, and B. Ai, "A survey on user-centric cell-free massive MIMO systems," *Digital Commun. Netw.*, vol. 8, no. 5, pp. 695–719, Dec. 2022.

[34] J. Kassam, D. Castanheira, A. a. Silva, R. Dinis, and A. Gameiro, "A review on cell-free massive MIMO systems," *Electronics*, vol. 12, no. 4, p. 1001, Feb. 2023.

[35] M. Mohammadi, Z. Mobini, H. Q. Ngo, and M. Matthaiou, "Next-generation multiple access with cell-free massive MIMO," *Proc. IEEE*, vol. 112, no. 9, pp. 1372–1420, Sept. 2024.

[36] A. Sabharwal, P. Schniter, D. Guo, D. W. Bliss, S. Rangarajan, and R. Wichman, "In-band full-duplex wireless: Challenges and opportunities," *IEEE J. Sel. Areas Commun.*, vol. 32, no. 9, pp. 1637–1652, Sept. 2014.

[37] Z. Zhang, K. Long, A. V. Vasilakos, and L. Hanzo, "Full-duplex wireless communications: Challenges, solutions, and future research directions," *Proc. IEEE*, vol. 104, no. 7, pp. 1369–1409, Jul. 2016.

[38] S. Goyal, P. Liu, S. S. Panwar, R. A. Difazio, R. Yang, and E. Bala, "Full duplex cellular systems: Will doubling interference prevent doubling capacity?" *IEEE Commun. Mag.*, vol. 53, no. 5, pp. 121–127, May 2015.

[39] M. Amjad, F. Akhtar, M. H. Rehmani, M. Reisslein, and T. Umer, "Full-duplex communication in cognitive radio networks: A survey," *IEEE Commun. Surveys Tuts.*, vol. 19, no. 4, pp. 2158–2191, Fourthquarter 2017.

[40] S. K. Sharma, T. E. Bogale, L. B. Le, S. Chatzinotas, X. Wang, and B. Ottersten, "Dynamic spectrum sharing in 5G wireless networks with full-duplex technology: Recent advances and research challenges," *IEEE Commun. Surveys Tuts.*, vol. 20, no. 1, pp. 674–707, Firstquarter 2018.

[41] M. Mohammadi *et al.*, "Full-duplex non-orthogonal multiple access for next generation wireless systems," *IEEE Commun. Mag.*, vol. 57, no. 5, pp. 110–116, May 2019.

[42] G. C. Alexandropoulos, M. A. Islam, and B. Smida, "Full-duplex massive multiple-input, multiple-output architectures: Recent advances, applications, and future directions," *IEEE Veh. Technol. Mag.*, pp. 2–10, Oct. 2022.

[43] B. Smida, A. Sabharwal, G. Fodor, G. C. Alexandropoulos, H. A. Suraweera, and C.-B. Chae, "Full-duplex wireless for 6G: Progress brings new opportunities and challenges," *IEEE J. Sel. Areas Commun.*, vol. 41, no. 9, pp. 2729–2750, Sept. 2023.

[44] M. Mohammadi, Z. Mobini, H. Q. Ngo, and M. Matthaiou, "Ten years of research advances in full-duplex massive MIMO," *IEEE Trans. Commun.*, vol. 73, no. 3, pp. 1756–1786, Mar. 2025.

[45] M. Mohammadi, Z. Mobini, D. Galappaththige, and C. Tellambura, "A comprehensive survey on full-duplex communication: Current solutions, future trends, and open issues," *IEEE Commun. Surveys Tuts.*, vol. 25, no. 4, pp. 2190–2244, Secondquarter 2023.

[46] X. Zhang, W. Cheng, and H. Zhang, "Full-duplex transmission in PHY and MAC layers for 5G mobile wireless networks," *IEEE Wireless Commun.*, vol. 22, no. 5, pp. 112–121, Oct. 2015.

[47] H. Q. Ngo, H. A. Suraweera, M. Matthaiou, and E. G. Larsson, "Multipair full-duplex relaying with massive arrays and linear processing," *IEEE J. Sel. Areas Commun.*, vol. 32, no. 9, pp. 1721–1737, Sept. 2014.

[48] H. Alves, T. Riihonen, and H. A. Suraweera, Eds., *Full-Duplex Communications for Future Wireless Networks*. Springer, 2020.

[49] M. Mohammadi, H. A. Suraweera, and C. Tellambura, "Uplink/downlink rate analysis and impact of power allocation for full-duplex cloud-RANs," *IEEE Trans. Wireless Commun.*, vol. 17, no. 9, pp. 5774–5788, Sept. 2018.

[50] T. Le-Ngoc and A. Masmoudi, *Full-Duplex Wireless Communications Systems: Self-Interference Cancellation*, 1st ed. Springer Publishing Company, Incorporated, 2017.

[51] B. Debaillie *et al.*, "In-band full-duplex transceiver technology for 5G mobile networks," in *Proc. IEEE ESSCIRC*, Sept. 2015, pp. 84–87.

[52] T. Kim, K. Min, and S. Park, "Self-interference channel training for full-duplex massive MIMO systems," *Sensors*, vol. 21, no. 9, p. 3250, May 2021.

[53] A. Sahai, G. Patel, and A. Sabharwal, "Pushing the limits of full-duplex: Design and real-time implementation," *arXiv*, vol. abs/1107.0607, 2011.

[54] X. Wu, Y. Shen, and Y. Tang, "The power delay profile of the single-antenna full-duplex self-interference channel in indoor environments at 2.6 GHz," *IEEE Antennas Wireless Propag. Lett.*, vol. 13, pp. 1561–1564, Aug. 2014.

[55] F. Chen, R. Morawski, and T. Le-Ngoc, "Self-interference channel characterization for wideband 2×2 MIMO full-duplex transceivers using dual-polarized antennas," *IEEE Trans. Antennas Propag.*, vol. 66, no. 4, pp. 1967–1976, Apr. 2018.

[56] Y. He, X. Yin, and H. Chen, "Spatiotemporal characterization of self-interference channels for 60-GHz full-duplex communication," *IEEE Antennas Wireless Propag. Lett.*, vol. 16, pp. 2220–2223, May 2017.

[57] C. Ziółkowski and J. M. Kelner, "Geometry-based statistical model for the temporal, spectral, and spatial characteristics of the land mobile channel," *Wireless Pers. Commun.*, vol. 83, no. 1, p. 631–652, Jul. 2015.

[58] J. C. Liberti and T. S. Rappaport, "A geometrically based model for line-of-sight multipath radio channels," in *Proc. IEEE VTC*, May 1996, pp. 844–848.

[59] Y. Chen and V. Dubey, "Accuracy of geometric channel-modeling methods," *IEEE Trans. Veh. Technol.*, vol. 53, no. 1, pp. 82–93, Jan. 2004.

[60] W. Wu, J. Zhuang, W. Wang, and B. Wang, "Geometry-based statistical channel models of reflected-path self-interference in full-duplex wireless," *IEEE Access*, vol. 7, pp. 48 778–48 791, Apr. 2019.

[61] B. P. Day, A. R. Margetts, D. W. Bliss, and P. Schniter, "Full-duplex bidirectional MIMO: achievable rates under limited dynamic range," *IEEE Trans. Signal Process.*, vol. 60, pp. 3702–3713, Jul. 2012.

[62] M. Duarte and A. Sabharwal, "Full-duplex wireless communications using off-the-shelf radios: Feasibility and first results," in *Proc. IEEE Asilomar CSSC*, Nov. 2010, pp. 1558–1562.

[63] D. Bharadia, E. McMilin, and S. Katti, "Full duplex radios," in *Proc. ACM SIGCOMM*, Aug. 2013, pp. 375–386.

[64] E. Aryafar, M. A. Khojastepour, K. Sundaresan, S. Rangarajan, and M. Chiang, "MIDU: Enabling MIMO full duplex," in *Proc. ACM MobiCom*, Aug. 2012, pp. 257–268.

[65] E. Everett, "Full-duplex infrastructure nodes: Achieving long range with half-duplex mobiles," Ph.D. dissertation, Rice University, Apr. 2012.

[66] M. A. Khojastepour, K. Sundaresan, S. Rangarajan, X. Zhang, and S. Barghi, "The case for antenna cancellation for scalable full-duplex wireless communications," in *Proc. ACM Workshop HotNets*, Nov. 2011.

[67] T. Snow, C. Fulton, and W. J. Chappell, "Transmit–receive duplexing using digital beamforming system to cancel self-interference," *IEEE Trans. Microw. Theory Techn.*, vol. 59, no. 12, pp. 3494–3503, Dec. 2011.

[68] T. Riihonen, S. Werner, and R. Wichman, "Mitigation of loopback self-interference in full-duplex MIMO relays," *IEEE Trans. Signal Process.*, vol. 59, no. 12, pp. 5983–5993, Dec. 2011.

[69] M. Duarte *et al.*, "Design and characterization of a full-duplex multi-antenna system for WiFi networks," *IEEE Trans. Veh. Technol.*, vol. 63, no. 3, pp. 1160–1177, Mar. 2014.

[70] T. Riihonen, A. Balakrishnan, K. Haneda, S. Wyne, S. Werner, and R. Wichman, "Optimal eigenbeamforming for suppressing self-interference in full-duplex MIMO relays," in *Proc. IEEE CISS*, Mar. 2011, pp. 1–6.

[71] M. Jain *et al.*, "Practical, real-time, full duplex wireless," in *Proc. ACM MobiCom*, Sept. 2011, p. 301–312.

[72] L. Scharf and C. Demeure, *Statistical Signal Processing: Detection, Estimation, and Time Series Analysis*. Addison-Wesley Publishing Company, 1991.

[73] A. Balatsoukas-Stimming, A. C. M. Austin, P. Belanovic, and A. Burg, "Baseband and RF hardware impairments in full-duplex wireless systems: Experimental characterisation and suppression," *EURASIP J. Wireless Commun. Netw.*, vol. 2015, pp. 1687–1499, May 2015.

[74] D. Korpi, L. Anttila, V. Syrjälä, and M. Valkama, "Widely linear digital self-interference cancellation in direct-conversion full-duplex transceiver," *IEEE J. Sel. Areas Commun.*, vol. 32, no. 9, pp. 1674–1687, Sept. 2014.

[75] A. Sahai, G. Patel, C. Dick, and A. Sabharwal, "On the impact of phase noise on active cancelation in wireless full-duplex," *IEEE Trans. Veh. Technol.*, vol. 62, no. 9, pp. 4494–4510, Nov. 2013.

[76] V. Syrjala, M. Valkama, L. Anttila, T. Riihonen, and D. Korpi, "Analysis of oscillator phase-noise effects on self-interference cancellation in full-duplex OFDM radio transceivers," *IEEE Trans. Wireless Commun.*, vol. 13, no. 6, pp. 2977–2990, Jun. 2014.

[77] D. Korpi, L. Anttila, and M. Valkama, "Nonlinear self-interference cancellation in MIMO full-duplex transceivers under crosstalk," *EURASIP J. Wireless Commun. Netw.*, vol. 2017, pp. 1–15, Feb. 2017.

[78] V. Raj and S. Kalyani, "Backpropagating through the air: Deep learning at physical layer without channel models," *IEEE Commun. Lett.*, vol. 22, no. 11, pp. 2278–2281, Nov. 2018.

[79] B. Smida, R. Wichman, K. E. Kolodziej, H. A. Suraweera, T. Riihonen, and A. Sabharwal, "In-band full-duplex: The physical layer," *Proc. IEEE*, vol. 112, no. 5, pp. 433–462, Aug. 2024.

[80] V. W. S. Wong, R. Schober, D. W. K. Ng, and L.-C. Wang, *Key Technologies for 5G Wireless Systems*. Cambridge University Press, 2017.

[81] S. Venkatesan, A. Lozano, and R. Valenzuela, "Network MIMO: Overcoming intercell interference in indoor wireless systems," in *Proc. IEEE Asilomar CSSC*, Nov. 2007, pp. 83–87.

[82] S. Shamai and B. Zaidel, "Enhancing the cellular downlink capacity via co-processing at the transmitting end," in *Proc. IEEE VTC*, May 2001, pp. 1745–1749.

[83] G. Caire, S. A. Ramprashad, and H. C. Papadopoulos, "Rethinking network MIMO: Cost of CSIT, performance analysis, and architecture comparisons," in *Proc. ITA Workshop*, Jan. 2010, pp. 1–10.

[84] O. Simeone, O. Somekh, H. V. Poor, and S. Shamai, "Distributed MIMO in multi-cell wireless systems via finite-capacity links," in *Proc. IEEE ISCCSP*, Mar. 2008, pp. 203–206.

[85] P. Marsch, S. Brück, A. Garavaglia, M. Schulist, R. Weber, and A. Dekorsy, "Clustering," in *Coordinated Multipoint in Mobile Communications*. Cambridge, UK: Cambridge University Press, 2011, p. 139–160.

[86] D. Galappaththige and G. Amarasuriya, "Cell-free massive MIMO with underlay spectrum-sharing," in *Proc. IEEE ICC*, May 2019, pp. 1–7.

[87] F. Rezaei, A. R. Heidarpour, C. Tellambura, and A. Tadaion, "Underlaid spectrum sharing for cell-free massive MIMO-NOMA," *IEEE Commun. Lett.*, vol. 24, no. 4, pp. 907–911, Apr. 2020.

[88] D. Galappaththige, R. Shrestha, and G. A. Aruma Baduge, "Exploiting cell-free massive MIMO for enabling simultaneous wireless information and power transfer," *IEEE Trans. Green Commun. Netw.*, vol. 5, no. 3, pp. 1541–1557, Sept. 2021.

[89] D. Galappaththige and G. Amarasuriya, "NOMA-aided cell-free massive MIMO with underlay spectrum-sharing," in *Proc. IEEE ICC*, Jun. 2020, pp. 1–6.

[90] F. Rezaei, C. Tellambura, A. A. Tadaion, and A. R. Heidarpour, "Rate analysis of cell-free massive MIMO-NOMA with three linear precoders," *IEEE Trans. Commun.*, vol. 68, no. 6, pp. 3480–3494, Jun. 2020.

[91] H. Huang, M. Trivellato, A. Hottinen, M. Shafi, P. J. Smith, and R. Valenzuela, "Increasing downlink cellular throughput with limited network MIMO coordination," *IEEE Trans. Wireless Commun.*, vol. 8, no. 6, pp. 2983–2989, Jun. 2009.

[92] J. Zhang, R. Chen, J. G. Andrews, A. Ghosh, and R. W. Heath Jr., "Networked MIMO with clustered linear precoding," *IEEE Trans. Wireless Commun.*, vol. 8, no. 4, pp. 1910–1921, Apr. 2009.

[93] P. Marsch and G. P. Fettweis, "On multicell cooperative transmission in backhaul-constrained cellular systems," *Ann. Telecommun. - Annales des Télécommun.*, vol. 63, pp. 253–269, May 2008.

[94] A. Osseiran, J. F. Monserrat, and W. Mohr, *Coordinated MultiPoint (CoMP) Systems*. Wiley, NJ, USA, 2011, pp. 121–155.

[95] E. Nayebi, A. Ashikhmin, T. L. Marzetta, H. Yang, and B. D. Rao, "Precoding and power optimization in cell-free massive MIMO systems," *IEEE Trans. Wireless Commun.*, vol. 16, no. 7, pp. 4445–4459, Jul. 2017.

[96] D. Galappaththige and C. Tellambura, "Sum rate maximization for RSMA-assisted CF mMIMO networks with SWIPT users," *IEEE Wireless Communications Letters*, vol. 13, no. 5, pp. 1300–1304, May 2024.

[97] E. Björnson, J. Hoydis, and L. Sanguinetti, *Massive MIMO Networks: Spectral, Energy, and Hardware Efficiency*, 2017, vol. 11.

[98] Z. Chen and E. Björnson, "Channel hardening and favorable propagation in cell-free massive MIMO with stochastic geometry," *IEEE Trans. Commun.*, vol. 66, no. 11, pp. 5205–5219, Nov. 2018.

[99] A. A. Polegre, F. Riera-Palou, G. Femenias, and A. G. Armada, "Channel hardening in cell-free and user-centric massive MIMO networks with spatially correlated Ricean fading," *IEEE Access*, vol. 8, pp. 139 827–139 845, Aug. 2020.

[100] T. T. Vu, D. T. Ngo, H. Q. Ngo, and T. Le-Ngoc, "Full-duplex cell-free massive MIMO," in *Proc. IEEE ICC*, May 2019, pp. 1–6.

[101] D. Wang, M. Wang, P. Zhu, J. Li, J. Wang, and X. You, "Performance of network-assisted full-duplex for cell-free massive MIMO," *IEEE Trans. Commun.*, vol. 68, no. 3, pp. 1464–1478, Mar. 2020.

[102] H. V. Nguyen *et al.*, "On the spectral and energy efficiencies of full-duplex cell-free massive MIMO," *IEEE J. Sel. Areas Commun.*, vol. 38, no. 8, pp. 1698–1718, Aug. 2020.

[103] S. Datta, D. N. Amudala, E. Sharma, R. Budhiraja, and S. S. Panwar, "Full-duplex cell-free massive MIMO systems: Analysis and decentralized optimization," *IEEE Open J. Commun. Society*, vol. 3, pp. 31–50, Feb. 2022.

[104] M. Mohammadi, T. T. Vu, B. Naderi Beni, H. Q. Ngo, and M. Matthaiou, "Virtually full-duplex cell-free massive MIMO with access point mode assignment," in *Proc. IEEE SPAWC*, Jul. 2022, pp. 1–5.

[105] P. Anokye, R. K. Ahiadormey, and K.-J. Lee, "Full-duplex cell-free massive MIMO with low-resolution ADCs," *IEEE Trans. Veh. Technol.*, vol. 70, no. 11, pp. 12 179–12 184, Nov. 2021.

[106] H. V. Nguyen *et al.*, "A novel heap-based pilot assignment for full duplex cell-free massive MIMO with zero-forcing," in *Proc. IEEE ICC*, Jun. 2020, pp. 1–6.

[107] S. Datta, E. Sharma, D. N. Amudala, R. Budhiraja, and S. S. Panwar, "FD cell-free mMIMO: Analysis and optimization," in *Proc. IEEE ICC*, Jun. 2021, pp. 1–6.

[108] D. Yu, Y. Liu, Z. Li, and H. Zhang, "Energy-efficient beamforming design for user-centric networks with full-duplex wireless fronthaul," *IEEE Trans. Commun.*, vol. 71, no. 3, pp. 1521–1535, Mar. 2023.

[109] S. Dey and R. Budhiraja, "FD cell-free massive MIMO systems with downlink pilots: Analysis and optimization," *IEEE Trans. Commun.*, vol. 70, no. 11, pp. 7591–7608, Nov. 2022.

[110] D. Deng *et al.*, "Flexible user duplexing in cell-free massive MIMO: A deep reinforcement learning approach," in *Proc. IEEE ICCC*, Aug. 2022, pp. 296–301.

[111] Q. Gao, M. Jia, Q. Guo, X. Gu, and L. Hanzo, "Jointly optimized beamforming and power allocation for full-duplex cell-free NOMA in space-ground integrated networks," *IEEE Trans. Commun.*, vol. 71, no. 5, pp. 2816–2830, May 2023.

[112] X. Lu, N. Cong Luong, D. T. Hoang, D. Niyato, Y. Xiao, and P. Wang, "Secure wirelessly powered networks at the physical layer: Challenges, countermeasures, and road ahead," *Proc. IEEE*, vol. 110, no. 1, pp. 193–209, Jan. 2022.

[113] H. Kim, *Wireless Communications Systems Design*. Wiley, 2015.

[114] M. K. Ozdemir and H. Arslan, "Channel estimation for wireless OFDM systems," *IEEE Commun. Surveys Tuts.*, vol. 9, no. 2, pp. 18–48, Secondquarter 2007.

[115] B. Hassibi and B. Hochwald, "How much training is needed in multiple-antenna wireless links?" *IEEE Trans. Inf. Theory*, vol. 49, no. 4, pp. 951–963, Apr. 2003.

[116] E. Björnson, E. G. Larsson, and M. Debbah, "Massive MIMO for maximal spectral efficiency: How many users and pilots should be allocated?" *IEEE Trans. Wireless Commun.*, vol. 15, no. 2, pp. 1293–1308, Feb. 2016.

[117] A. Chowdhury, R. Chopra, and C. R. Murthy, "Can dynamic TDD enabled half-duplex cell-free massive MIMO outperform full-duplex cellular massive MIMO?" *IEEE Trans. Commun.*, vol. 70, no. 7, pp. 4867–4883, Jul. 2022.

[118] Y. Hu, H. Ge, H. Wang, and D. Wang, "Spectral efficiency of network-assisted full-duplex for cell-free massive MIMO system under pilot contamination," *IEEE Access*, vol. 9, pp. 110 826–110 841, Aug. 2021.

[119] "3GPP TR 36.814, further advancements for E-UTRA physical layer aspects, V.9.0.0 Rel. 9," Mar. 2010. Available Online: https://portal.3gpp.org/desktopmodules/Specifications/SpecificationDetails.aspx?specificationId=2493.

[120] H. Q. Ngo, L.-N. Tran, T. Q. Duong, M. Matthaiou, and E. G. Larsson, "On the total energy efficiency of cell-free massive MIMO," *IEEE Trans. Green Commun. Netw.*, vol. 2, no. 1, pp. 25–39, Mar. 2018.

[121] P. Anokye, D. K. P. Asiedu, and K.-J. Lee, "Power optimization of cell-free massive MIMO with full-duplex and low-resolution ADCs," *IEEE Trans. Wireless Commun.*, vol. 22, no. 10, pp. 6706–6723, Oct. 2023.

[122] E. Björnson, E. A. Jorswieck, M. Debbah, and B. Ottersten, "Multiobjective signal processing optimization: The way to balance conflicting metrics in 5G systems," *IEEE Signal Process. Mag.*, vol. 31, no. 6, pp. 14–23, Oct. 2014.

[123] H. Haas and S. McLaughlin, "A dynamic channel assignment algorithm for a hybrid TDMA/CDMA-TDD interface using the novel TS-opposing technique," *IEEE J. Sel. Areas Commun.*, vol. 19, no. 10, pp. 1831–1846, Oct. 2001.

[124] J. Liu, S. Han, W. Liu, and C. Yang, "The value of full-duplex for cellular networks: A hybrid duplex-based study," *IEEE Trans. Commun.*, vol. 65, no. 12, pp. 5559–5573, Dec. 2017.

[125] J. Li, A. Huang, H. Shan, H. H. Yang, and T. Q. S. Quek, "Analysis of packet throughput in small cell networks under clustered dynamic TDD," *IEEE Trans. Wireless Commun.*, vol. 17, no. 9, pp. 5729–5742, Sept. 2018.

[126] Z. Shen, A. Khoryaev, E. Eriksson, and X. Pan, "Dynamic uplink-downlink configuration and interference management in TD-LTE," *IEEE Commun. Mag.*, vol. 50, no. 11, pp. 51–59, Nov. 2012.

[127] H. Thomsen, P. Popovski, E. d. Carvalho, N. K. Pratas, D. M. Kim, and F. Boccardi, "CoMPflex: CoMP for in-band wireless full duplex," *IEEE Wireless Commun. Lett.*, vol. 5, no. 2, pp. 144–147, Apr. 2016.

[128] Y. Xin, R. Zhang, D. Wang, J. Li, L. Yang, and X. You, "Antenna clustering for bidirectional dynamic network with large-scale distributed antenna systems," *IEEE Access*, vol. 5, pp. 4037–4047, Apr. 2017.

[129] J. Li, Q. Lv, P. Zhu, D. Wang, J. Wang, and X. You, "Network-assisted full-duplex distributed massive MIMO systems with beamforming training based CSI estimation," *IEEE Trans. Wireless Commun.*, vol. 20, no. 4, pp. 2190–2204, Apr. 2021.

[130] M. Mohammadi, T. T. Vu, H. Q. Ngo, and M. Matthaiou, "Network-assisted full-duplex cell-free massive MIMO: Spectral and energy efficiencies," *IEEE J. Sel. Areas Commun.*, vol. 41, no. 9, pp. 2833–2851, Sept. 2023.

[131] Y. Zhu, J. Li, P. Zhu, H. Wu, D. Wang, and X. You, "Optimization of duplex mode selection for network-assisted full-duplex cell-free massive MIMO systems," *IEEE Commun. Lett.*, vol. 25, no. 11, pp. 3649–3653, Nov. 2021.

[132] X. Sun *et al.*, "Hierarchical reinforcement learning for AP duplex mode optimization in network-assisted full-duplex cell-free networks," *IEEE Syst. J.*, vol. 17, no. 4, pp. 6540–6551, Dec. 2023.

[133] X. Xia *et al.*, "Joint uplink power control, downlink beamforming, and mode selection for secrecy cell-free massive MIMO with network-assisted full duplexing," *IEEE Syst. J.*, vol. 17, no. 1, pp. 720–731, Mar. 2023.

[134] ——, "Joint user selection and transceiver design for cell-free with network-assisted full duplexing," *IEEE Trans. Wireless Commun.*, vol. 20, no. 12, pp. 7856–7870, Dec. 2021.

[135] X. Xia, D. Wang, J. Zhao, Z. Zhang, and X. You, "Joint energy harvesting and transmission optimization for cell-free massive MIMO with network-assisted full duplexing," *IEEE Trans. Veh. Technol.*, vol. 72, no. 6, pp. 7439–7453, Jun. 2023.

[136] Y. Zhu, J. Li, P. Zhu, D. Wang, H. Ye, and X. You, "Load-aware dynamic mode selection for network-assisted full-duplex cell-free large-scale distributed MIMO systems," *IEEE Access*, vol. 10, pp. 22 301–22 310, Mar. 2022.

[137] T. T. Vu, H. Q. Ngo, M. N. Dao, and E. G. Larsson, "Multipair DF relaying with network-assisted full-duplex cell-free massive MIMO," in *Proc. IEEE EUSIPCO*, Sept. 2023, pp. 1474–1478.

[138] M. Mohammadi, L.-N. Tran, Z. Mobini, H. Q. Ngo, and M. Matthaiou, "Cell-free massive MIMO and SWIPT: Access point operation mode selection and power control," in *Proc. IEEE GLOBECOM*, Dec. 2023, pp. 661–666.

[139] ——, "Cell-free massive MIMO-assisted SWIPT for IoT networks," *IEEE Trans. Wireless Commun.*, 2025, Accepted.

[140] Z. Mobini, H. Q. Ngo, M. Matthaiou, and L. Hanzo, "Cell-free massive MIMO surveillance of multiple untrusted communication links," *IEEE Internet Things J.*, vol. 11, no. 20, pp. 33 010–33 026, Oct. 2024.

[141] E. Björnson, L. Sanguinetti, J. Hoydis, and M. Debbah, "Optimal design of energy-efficient multi-user MIMO systems: Is massive MIMO the answer?" *IEEE Trans. Wireless Commun.*, vol. 14, no. 6, pp. 3059–3075, June 2015.

[142] E. Björnson and L. Sanguinetti, "Making cell-free massive MIMO competitive with MMSE processing and centralized implementation," *IEEE Trans. Wireless Commun.*, vol. 19, no. 1, pp. 77–90, Jan. 2020.

[143] A. Alkhateeb, J. Mo, N. Gonzalez-Prelcic, and R. W. Heath Jr., "MIMO precoding and combining solutions for millimeter-wave systems," *IEEE Commun. Mag.*, vol. 52, no. 12, pp. 122–131, Dec. 2014.

[144] S. Sun, T. S. Rappaport, R. W. Heath Jr., A. Nix, and S. Rangan, "MIMO for millimeter-wave wireless communications: Beamforming, spatial multiplexing, or both?" *IEEE Commun. Mag.*, vol. 52, no. 12, pp. 110–121, Dec. 2014.

[145] Z. Xiao, T. He, P. Xia, and X.-G. Xia, "Hierarchical codebook design for beamforming training in millimeter-wave communication," *IEEE Trans. Wireless Commun.*, vol. 15, no. 5, pp. 3380–3392, May 2016.

[146] Z. Xiao, P. Xia, and X.-G. Xia, "Full-duplex millimeter-wave communication," *IEEE Wireless Commun.*, vol. 24, no. 6, pp. 136–143, Dec. 2017.

[147] K. Satyanarayana, M. El-Hajjar, P.-H. Kuo, A. Mourad, and L. Hanzo, "Hybrid beamforming design for full-duplex millimeter wave communication," *IEEE Trans. Veh. Technol.*, vol. 68, no. 2, pp. 1394–1404, Feb. 2019.

[148] I. P. Roberts, A. Chopra, T. Novlan, S. Vishwanath, and J. G. Andrews, "STEER: Beam selection for full-duplex millimeter wave communication systems," *IEEE Trans. Commun.*, vol. 70, no. 10, pp. 6902–6917, Oct. 2022.

[149] L. Li, K. Josiam, and R. Taori, "Feasibility study on full-duplex wireless millimeter-wave systems," in *Proc. IEEE ICASSP*, May 2014, pp. 2769–2773.

[150] A. Demir, T. Haque, E. Bala, and P. Cabrol, "Exploring the possibility of full-duplex operations in mmWave 5G systems," in *Proc. IEEE WAMICON*, Apr. 2016, pp. 1–5.

[151] S. Rajagopal, R. Taori, and S. Abu-Surra, "Self-interference mitigation for in-band mmWave wireless backhaul," in *Proc. IEEE CCNC*, Jan. 2014, pp. 551–556.

[152] C. B. Barneto, T. Riihonen, S. D. Liyanaarachchi, M. Heino, N. González-Prelcic, and M. Valkama, "Beamformer design and optimization for joint communication and full-duplex sensing at mm-Waves," *IEEE Trans. Commun.*, vol. 70, no. 12, pp. 8298–8312, Dec. 2022.

[153] G. Femenias and F. Riera-Palou, "Cell-free millimeter-wave massive MIMO systems with limited fronthaul capacity," *IEEE Access*, vol. 7, pp. 44 596–44 612, Apr. 2019.

[154] S. Fukue, G. T. Freitas de Abreu, and K. Ishibashi, "Network-assisted full-duplex millimeter-wave cell-free massive MIMO with localization-aided inter-user channel estimation," in *Proc. IEEE ICION*, Jan. 2023, pp. 13–18.

[155] J. Li *et al.*, "Network-assisted full-duplex cell-free mmWave massive MIMO systems with DAC quantization and fronthaul compression," *ArXiv*, vol. abs/2302.05571, 2023.

[156] B. Li, Z. Fei, and Y. Zhang, "UAV communications for 5G and beyond: Recent advances and future trends," *IEEE Internet Things J.*, vol. 6, no. 2, pp. 2241–2263, Apr. 2019.

[157] M. Mozaffari, W. Saad, M. Bennis, Y.-H. Nam, and M. Debbah, "A tutorial on UAVs for wireless networks: Applications, challenges, and open problems," *IEEE Commun. Surveys Tuts.*, vol. 21, no. 3, pp. 2334–2360, Thirdquarter 2019.

[158] H. Wang, J. Wang, G. Ding, J. Chen, Y. Li, and Z. Han, "Spectrum sharing planning for full-duplex UAV relaying systems with underlaid D2D communications," *IEEE J. Sel. Areas Commun.*, vol. 36, no. 9, pp. 1986–1999, Sept. 2018.

[159] Q. Song, F.-C. Zheng, Y. Zeng, and J. Zhang, "Joint beamforming and power allocation for UAV-enabled full-duplex relay," *IEEE Trans. Veh. Technol.*, vol. 68, no. 2, pp. 1657–1671, Feb. 2019.

[160] M. Hua, L. Yang, C. Pan, and A. Nallanathan, "Throughput maximization for full-duplex UAV aided small cell wireless systems," *IEEE Wireless Commun. Lett.*, vol. 9, no. 4, pp. 475–479, Apr. 2020.

[161] W. Shi *et al.*, "Joint UL/DL resource allocation for UAV-aided full-duplex NOMA communications," *IEEE Trans. Wireless Commun.*, vol. 69, no. 12, pp. 8474–8487, Dec. 2021.

[162] M. Katwe, K. Singh, P. K. Sharma, C.-P. Li, and Z. Ding, "Dynamic user clustering and optimal power allocation in UAV-assisted full-duplex hybrid NOMA system," *IEEE Trans. Wireless Commun.*, vol. 21, no. 4, pp. 2573–2590, Apr. 2022.

[163] C. Liu, J. Lee, and T. Q. S. Quek, "Safeguarding UAV communications against full-duplex active eavesdropper," *IEEE Trans. Wireless Commun.*, vol. 18, no. 6, pp. 2919–2931, Jun. 2019.

[164] L. Zhu, J. Zhang, Z. Xiao, X. Cao, X.-G. Xia, and R. Schober, "Millimeter-wave full-duplex UAV relay: Joint positioning, beamforming, and power control," *IEEE J. Sel. Areas Commun.*, vol. 38, no. 9, pp. 2057–2073, Sept. 2020.

[165] L. Zhang, Q. Fan, and N. Ansari, "3-D drone-base-station placement with in-band full-duplex communications," *IEEE Commun. Lett.*, vol. 22, no. 9, pp. 1902–1905, Sept. 2018.

[166] J. Zheng, J. Zhang, and B. Ai, "Wireless power transfer for UAV communications with cell-free massive MIMO systems," in *Proc. IEEE Int. Conf. Commun.*, Jun. 2021, pp. 1–6.

[167] ——, "UAV communications with WPT-aided cell-free massive MIMO systems," *IEEE J. Sel. Areas Commun.*, vol. 39, no. 10, pp. 3114–3128, Oct. 2021.

[168] C. Liu, W. Feng, Y. Chen, C.-X. Wang, and N. Ge, "Cell-free satellite-UAV networks for 6G wide-area internet of things," *IEEE J. Sel. Areas Commun.*, vol. 39, no. 4, pp. 1116–1131, Apr. 2021.

[169] Z. Wu and Q. Wang, "Trajectory optimization and power allocation for cell-free satellite-UAV Internet of things," *IEEE Access*, vol. 11, pp. 203–213, Jan. 2023.

[170] B. Al-Nahhas, A. Chaaban, and M. J. Hossain, "Improving UAV communication in cell free MIMO using a reconfigurable intelligent surface," in *Proc. IEEE GLOBECOM*, Dec. 2022, pp. 1152–1157.

[171] C. Diaz-Vilor, A. Lozano, and H. Jafarkhani, "Cell-free UAV networks with wireless fronthaul: Analysis and optimization," *IEEE Trans. Wireless Commun.*, vol. 23, no. 3, pp. 2054–2069, Mar. 2023.

[172] C. D'Andrea, A. Garcia-Rodriguez, G. Geraci, L. G. Giordano, and S. Buzzi, "Analysis of UAV communications in cell-free massive mimo systems," *IEEE Open J. Commun. Soc.*, vol. 1, pp. 133–147, Jan. 2020.

[173] Z. Wan *et al.*, "Performance of cellular-connected UAV in cell-free radio access network with network-assisted full-duplex," *IEEE Trans. Wireless Commun.*, vol. 23, no. 10, pp. 14 848–14 863, Oct. 2024.

[174] Z. Wan, J. Li, P. Zhu, D. Wang, F. Liu, and X. You, "Performance analysis of multi-UAV aided cell-free radio access network with network-assisted full-duplex for URLLC," *IEEE Trans. Commun.*, vol. 72, no. 9, pp. 5810–5822, Sept. 2024.

[175] J. Li *et al.*, "Optimization of node duplex mode for network-assisted full-duplex low-altitude CF-RAN systems with UAVs," *IEEE Internet Things J.*, vol. 11, no. 12, pp. 21 996–22 006, Jun. 2024.

[176] Q. Wu, S. Zhang, B. Zheng, C. You, and R. Zhang, "Intelligent reflecting surface-aided wireless communications: A tutorial," *IEEE Trans. Commun.*, vol. 69, no. 5, pp. 3313–3351, May 2021.

[177] D. Galappaththige, D. Kudathanthirige, and G. Amarasuriya, "Performance analysis of distributed intelligent reflective surface aided communications," in *Proc. IEEE GLOBECOM*, Dec. 2020, pp. 1–6.

[178] D. Galappaththige, F. Rezaei, C. Tellambura, and S. Herath, "RIS-empowered ambient backscatter communication systems," *IEEE Wireless Commun. Lett.*, vol. 12, no. 1, pp. 173–177, Jan. 2023.

[179] D. Galappaththige, D. Kudathanthirige, and G. Amarasuriya, "Performance analysis of IRS-assisted cell-free communication," in *Proc. IEEE GLOBECOM*, Dec. 2021, pp. 1–6.

[180] C. Huang, A. Zappone, G. C. Alexandropoulos, M. Debbah, and C. Yuen, "Reconfigurable intelligent surfaces for energy efficiency in wireless communication," *IEEE Trans. Wireless Commun.*, vol. 18, no. 8, pp. 4157–4170, Aug. 2019.

[181] M. Poulakis, "6G's metamaterials solution: There's plenty of bandwidth available if we use reconfigurable intelligent surfaces," *IEEE Spectr.*, vol. 59, no. 11, pp. 40–45, Nov. 2022.

[182] S. Hu, F. Rusek, and O. Edfors, "Beyond massive MIMO: The potential of data transmission with large intelligent surfaces," *IEEE Trans. Signal Process.*, vol. 66, no. 10, pp. 2746–2758, May 2018.

[183] T.-H. Vu and S. Kim, "Performance analysis of full-duplex two-way RIS-based systems with imperfect CSI and discrete phase-shift design," *IEEE Commun. Lett.*, vol. 27, no. 2, pp. 512–516, Feb. 2023.

[184] C. N. Efrem and I. Krikidis, "Joint IRS location and size optimization in multi-IRS aided two-way full-duplex communication systems," *IEEE Trans. Wireless Commun.*, vol. 22, no. 10, pp. 6518–6533, Oct. 2023.

[185] A. Bazrafkan, M. Poposka, Z. Hadzi-Velkov, P. Popovski, and N. Zlatanov, "Performance comparison between a simple full-duplex multi-antenna relay and a passive reflecting intelligent surface," *IEEE Trans. Wireless Commun.*, vol. 22, no. 8, pp. 5461–5472, Aug. 2023.

[186] M. Elhattab, M. A. Arfaoui, C. Assi, and A. Ghrayeb, "Reconfigurable intelligent surface enabled full-duplex/half-duplex cooperative non-orthogonal multiple access," *IEEE Trans. Wireless Commun.*, vol. 21, no. 5, pp. 3349–3364, May 2022.

[187] T. V. Chien, H. Q. Ngo, S. Chatzinotas, M. Di Renzo, and B. Ottersten, "Reconfigurable intelligent surface-assisted cell-free massive MIMO systems over spatially-correlated channels," *IEEE Trans. Wireless Commun.*, vol. 21, no. 7, pp. 5106–5128, Jul. 2022.

[188] N. T. Nguyen, V.-D. Nguyen, H. V. Nguyen, H. Q. Ngo, S. Chatzinotas, and M. Juntti, "Spectral efficiency analysis of hybrid relay-reflecting intelligent surface-assisted cell-free massive MIMO systems," *IEEE Trans. Wireless Commun.*, vol. 22, no. 5, pp. 3397–3416, May 2023.

[189] T. D. Hua, M. Mohammadi, H. Q. Ngo, and M. Matthaiou, "Cell-free massive MIMO SWIPT with beyond diagonal reconfigurable intelligent surfaces," in *Proc. IEEE WCNC*, Apr. 2024, pp. 1–6.

[190] "Framework and overall objectives of the future development of IMT for 2030 and beyond," ITU, Tech. Rep., June 2023, dRAFT NEW RECOMMENDATION.

[191] D. Galappaththige, M. Mohammadi, G. A. Baduge, and C. Tellambura, "Cell-free integrated sensing and communication: Principles, advances, and future directions," *arXiv preprint arXiv:2502.20345*, 2025, https://arxiv.org/abs/2502.20345.

[192] S. Zargari, D. Galappaththige, C. Tellambura, and G. Y. Li, "Downlink beamforming for cell-free ISAC: A fast complex oblique manifold approach," *IEEE Trans. Wireless Commun.*, pp. 1–1, 2025.

[193] F. Liu *et al.*, "Integrated sensing and communications: Toward dual-functional wireless networks for 6G and beyond," *IEEE J. Sel. Areas Commun.*, vol. 40, no. 6, pp. 1728–1767, Jun. 2022.

[194] A. Liu *et al.*, "A survey on fundamental limits of integrated sensing and communication," *IEEE Commun. Surveys Tuts.*, vol. 24, no. 2, pp. 994–1034, Secondquarter 2022.

[195] D. Galappaththige, S. Zargari, C. Tellambura, and G. Y. Li, "Near-field ISAC: Beamforming for multi-target detection," *IEEE Wireless Commun. Lett.*, vol. 13, no. 7, pp. 1938–1942, Jul. 2024.

[196] A. Hakimi, D. Galappaththige, and C. Tellambura, "A roadmap for NF-ISAC in 6G: A comprehensive overview and tutorial," *Entropy*, vol. 26, no. 9, Sept. 2024.

[197] S. Zargari, D. Galappaththige, C. Tellambura, and H. V. Poor, "A Riemannian manifold approach to constrained resource allocation in ISAC," *IEEE Trans. Commun.*, vol. 73, no. 5, pp. 3655–3670, May 2025.

[198] X. Liu, T. Huang, N. Shlezinger, Y. Liu, J. Zhou, and Y. C. Eldar, "Joint transmit beamforming for multiuser MIMO communications and MIMO radar," *IEEE Trans. Signal Process.*, vol. 68, pp. 3929–3944, Jun. 2020.

[199] F. Liu, W. Yuan, C. Masouros, and J. Yuan, "Radar-assisted predictive beamforming for vehicular links: Communication served by sensing," *IEEE Trans. Wireless Commun.*, vol. 19, no. 11, pp. 7704–7719, Nov. 2020.

[200] A. Bazzi and M. Chafii, "On outage-based beamforming design for dual-functional radar-communication 6G systems," *IEEE Trans. Wireless Commun.*, vol. 22, no. 8, pp. 5598–5612, Aug. 2023.

[201] D. Galappaththige, C. Tellambura, and A. Maaref, "Integrated sensing and backscatter communication," *IEEE Wireless Commun. Lett.*, vol. 12, no. 12, pp. 2043–2047, Dec. 2023.

[202] W. Mao, Y. Lu, C.-Y. Chi, B. Ai, Z. Zhong, and Z. Ding, "Communication-sensing region for cell-free massive MIMO ISAC systems," *IEEE Trans. Wireless Commun.*, vol. 23, no. 9, pp. 12 396–12 411, Sept. 2024.

[203] Z. Behdad, O. T. Demir, K. W. Sung, E. Björnson, and C. Cavdar, "Multi-static target detection and power allocation for integrated sensing and communication in cell-free massive MIMO," *IEEE Trans. Wireless Commun.*, vol. 23, no. 9, pp. 11 580–11 596, Sept. 2024.

[204] M. Elfiatoure, M. Mohammadi, H. Q. Ngo, H. Shin, and M. Matthaiou, "Multiple-target detection in cell-free massive MIMO-assisted ISAC," *IEEE Trans. Wireless Commun.*, vol. 24, no. 5, pp. 4283–4298, May, 2025.

[205] N. Athreya, V. Raj, and S. Kalyani, "Beyond 5G: Leveraging cell free TDD massive MIMO using cascaded deep learning," *IEEE Wireless Commun. Lett.*, vol. 9, no. 9, pp. 1533–1537, Sept. 2020.

[206] M. Bashar *et al.*, "Exploiting deep learning in limited-fronthaul cell-free massive MIMO uplink," *IEEE J. Sel. Areas Commun.*, vol. 38, no. 8, pp. 1678–1697, Aug. 2020.

[207] Y. Al-Eryani, M. Akrout, and E. Hossain, "Multiple access in cell-free networks: Outage performance, dynamic clustering, and deep reinforcement learning-based design," *IEEE J. Sel. Areas Commun.*, vol. 39, no. 4, pp. 1028–1042, Apr. 2021.

[208] Y. Al-Eryani and E. Hossain, "Self-organizing mmWave MIMO cell-free networks with hybrid beamforming: A hierarchical DRL-based design," *IEEE Trans. Commun.*, vol. 70, no. 5, pp. 3169–3185, Nov. 2022.

[209] I. P. Roberts, A. Chopra, T. Novlan, S. Vishwanath, and J. G. Andrews, "Spatial and statistical modeling of multi-panel millimeter wave self-interference," *IEEE J. Sel. Areas Commun.*, vol. 41, no. 9, p. 2780–2795, Sept. 2023.

[210] L. Liu, E. G. Larsson, W. Yu, P. Popovski, C. Stefanovic, and E. de Carvalho, "Sparse signal processing for grant-free massive connectivity: A future paradigm for random access protocols in the Internet of Things," *IEEE Signal Process. Mag.*, vol. 35, no. 5, pp. 88–99, Aug. 2018.

[211] Q. Zhang, J. Zhang, and S. Jin, "Grant-free random access in cell-free massive MIMO systems with UE detection thresholds: A stochastic geometry approach," *IEEE Trans. Veh. Technol.*, vol. 72, no. 6, pp. 8117–8121, Jun. 2023.
[212] Z. H. Shaik and E. G. Larsson, "Decentralized algorithms for out-of-system interference suppression in distributed MIMO," *IEEE Wireless Commun. Lett.*, vol. 13, no. 7, pp. 1953–1957, Jul. 2024.
[213] Z. H. Shaik, E. Björnson, and E. G. Larsson, "Distributed computation of a posteriori bit likelihood ratios in cell-free massive MIMO," in *Proc. IEEE EUSIPCO*, Aug. 2021, pp. 935–939.
[214] D. Galappaththige, S. Zargari, C. Tellambura, and G. Y. Li, "Optimization of rate-splitting multiple access with integrated sensing and backscatter communication," *IEEE Trans. Veh. Technol.*, vol. 74, no. 6, pp. 9117–9133, Jun. 2025.

Diluka Galappaththige (S'17–M'22) is a postdoctoral research fellow at the Department of Electrical and Computer Engineering, University of Alberta, Canada. He received his B.Sc. degree (First-class honor) in Electrical and Electronic Engineering from the Department of Electrical and Electronic Engineering, University of Peradeniya, Sri Lanka, in 2017, and his Ph.D. in Electrical and Computer Engineering from the School of Electrical, Computer, and Biomedical Engineering, Southern Illinois University, Carbondale, IL, USA, in 2021.

Dr. Galappaththige has been awarded a post-doctoral fellowship from NSERC for the academic year 2024-2026. His current research interests include, but are not limited to, the design, modeling, and analysis of massive multiple-input multiple-output (mMIMO) communication (i.e., including co-located mMIMO and cell-free/distributed mMIMO), full-duplex communication (FD), backscatter communication (BackCom), reconfigurable intelligent surfaces (RISs), integrated sensing and communication (ISAC), near-field ISAC, wireless power transfer, machine learning for wireless communication, signal processing, and emerging technologies for enabling fifth-generation (5G) and beyond wireless networks. He has authored or co-authored over 40 research articles in peer-reviewed journals and conferences in the area of wireless communication and signal processing. He was a recipient of the Exemplary Reviewer Award for IEEE Wireless Communications Letters (TWCL) in 2020 and IEEE Communications Letters (TCL) in 2021. He is currently an Associate Editor for IEEE Canadian Journal of Electrical and Computer Engineering and a Guest Editor for Symmetry and Entropy journals. He has actively served as a reviewer for many IEEE journals and conferences.

Mohammadali Mohammadi (S'09–M'15–SM'23) is currently a Lecturer at the Centre for Wireless Innovation (CWI), Queen's University Belfast, U.K. He previously held the position of Research Fellow at CWI from 2021 to 2024. His research interests include signal processing for wireless communications, cell-free massive MIMO, wireless power transfer, OTFS modulation, reconfigurable intelligent surfaces, and full-duplex communication. He has published more than 80 research papers in accredited international peer reviewed journals and conferences in the area of wireless communication and has co-authored two invited book chapters. He serves as an Associate Editor for IEEE Communications Letters and IEEE Open Journal of the Communications Society. He was a recipient of the Exemplary Reviewer Award for IEEE Transactions on Communications in 2020 and 2022, and IEEE Communications Letters in 2023. He has been a member of Technical Program Committees for many IEEE conferences, such as ICC, GLOBECOM, and VTC.

Hien Quoc Ngo (Fellow, IEEE) is currently a Reader with Queen's University Belfast, U.K. His main research interests include massive MIMO systems, cell-free massive MIMO, integreates sensing and communications, reconfigurable intelligent surfaces, and physical layer security. He has co-authored many research papers in wireless communications and co-authored the Cambridge University Press textbook *Fundamentals of Massive MIMO* (2016).

He received the IEEE ComSoc Stephen O. Rice Prize in 2015, the IEEE ComSoc Leonard G. Abraham Prize in 2017, the Best Ph.D. Award from EURASIP in 2018, and the IEEE CTTC Early Achievement Award in 2023. He also received the IEEE Sweden VT-COM-IT Joint Chapter Best Student Journal Paper Award in 2015. He was awarded the UKRI Future Leaders Fellowship in 2019. He serves as the Editor for the IEEE Transactions on Wireless Communications, IEEE Transactions on Communications, the Digital Signal Processing, and the Physical Communication (Elsevier). He was an Editor of the IEEE Wireless Communications Letters, a Guest Editor of IET Communications, and a Guest Editor of IEEE ACCESS in 2017.

Michail Matthaiou (Fellow, IEEE) obtained his Ph.D. degree from the University of Edinburgh, U.K. in 2008. He is currently a Professor of Communications Engineering and Signal Processing and Deputy Director of the Centre for Wireless Innovation (CWI) at Queen's University Belfast, U.K. He is also an Eminent Scholar at the Kyung Hee University, Republic of Korea. He has held research/faculty positions at Munich University of Technology (TUM), Germany and Chalmers University of Technology, Sweden. His research interests span signal processing for wireless communications, beyond massive MIMO, reflecting intelligent surfaces, mm-wave/THz systems and AI-empowered communications.

Dr. Matthaiou and his coauthors received the IEEE Communications Society (ComSoc) Leonard G. Abraham Prize in 2017. He currently holds the ERC Consolidator Grant BEATRICE (2021-2026) focused on the interface between information and electromagnetic theories. To date, he has received the prestigious 2023 Argo Network Innovation Award, the 2019 EURASIP Early Career Award and the 2018/2019 Royal Academy of Engineering/The Leverhulme Trust Senior Research Fellowship. His team was also the Grand Winner of the 2019 Mobile World Congress Challenge. He was the recipient of the 2011 IEEE ComSoc Best Young Researcher Award for the Europe, Middle East and Africa Region and a co-recipient of the 2006 IEEE Communications Chapter Project Prize for the best M.Sc. dissertation in the area of communications. He has co-authored papers that received best paper awards at the 2018 IEEE WCSP and 2014 IEEE ICC. In 2014, he received the Research Fund for International Young Scientists from the National Natural Science Foundation of China. He is currently the Editor-in-Chief of Elsevier Physical Communication, a Senior Editor for IEEE WIRELESS COMMUNICATIONS LETTERS and IEEE SIGNAL PROCESSING MAGAZINE, an Area Editor for IEEE TRANSACTIONS ON COMMUNICATIONS and Editor-in-Large for IEEE OPEN JOURNAL OF THE COMMUNICATIONS SOCIETY. He is an IEEE and AAIA Fellow.

Chintha Tellambura (Fellow, IEEE) received the B.Sc. degree (First class) in electrical and electronic engineering from the University of Moratuwa, Sri Lanka, the M.Sc. degree in electrical engineering from King's College, University of London, and the Ph.D. degree in electrical engineering from the University of Victoria, Canada. He was with Monash University, Australia, from 1997 to 2002. Dr. Tellambura is a Professor in the Department of Electrical and Computer Engineering at the University of Alberta. He has authored or co-authored over 650 journals and conference papers, demonstrating his expertise in the field. According to Google Scholar, his exceptional scholarly contributions have earned him an impressive H-index of 84. Dr. Tellambura has made significant contributions to various areas of research, including future wireless networks, machine learning for wireless networks, and signal processing.

Recognizing his outstanding accomplishments, he was elected as an IEEE Fellow in 2011 for his noteworthy contributions to physical layer wireless communication theory. In 2017, he was further honored as a fellow of the Canadian Academy of Engineering, a testament to his exceptional achievements. His dedication and expertise have been acknowledged through prestigious awards, including the Best Paper Awards in the Communication Theory Symposium in 2012, the IEEE International Conference on Communications (ICC) held in Canada in 2017, and another ICC in France. Moreover, Dr. Tellambura has been honored with the esteemed McCalla Professorship and the Killam Annual Professorship by the University of Alberta, further underscoring his significant impact on academia. Dr. Tellambura has also played a vital role in editorial responsibilities within the IEEE community. He served as an Editor for the IEEE Transactions on Communications from 1999 to 2011 and for the IEEE Transactions on Wireless Communications from 2001 to 2007. In the latter role, he was Area Editor of Wireless Communications Systems and Theory from 2007 to 2012, contributing to advancing the field through his editorial expertise.